AD-A046 092 MATHEMATICAL APPLICATIONS GROUP INC ELMSFORD N Y F/G 18/3
ENERGY DEPOSITION RATES AND COMPTON ELECTRON CURRENTS FROM LOW---ETC(U)
SEP 77 H S SCHECHTER, M O COHEN DAAG39-77-C-0020
UNCLASSIFIED MR-7054 HDL-CR-77-020 NL

| OF |

AD
A046092

END
DATE
FILMED
12-77
DDC

HDL-CR- 77-020-1

Energy Deposition Rates and Compton Electron Currents from Low-Altitude Bursts as a Function of Source Energy

November 1977

Prepared by

Mathematical Applications Group, Inc.
3 Westchester Plaza
Elmsford, N. Y. 10523

Under Contract

DAAG39-77-C-0020

U.S. Army Materiel Development and Readiness Command

HARRY DIAMOND LABORATORIES

Adelphi, Maryland 20783

UNCLASSIFIED (9) Interim rept. 17 Nov 76-1 Nov 77,

SECURITY CLASSIFICATION OF THIS PAGE (When Data Entered)

(19) REPORT DOCUMENTATION PAGE

READ INSTRUCTIONS BEFORE COMPLETING FORM

1. REPORT NUMBER (18) HDL-CR-77-020	2. GOVT ACCESSION NO.	3. RECIPIENT'S CATALOG NUMBER
4. TITLE (and Subtitle) (6) ENERGY DEPOSITION RATES AND COMPTON ELECTRON CURRENTS FROM LOW-ALTITUDE BURSTS AS A FUNCTION OF SOURCE ENERGY.		5. TYPE OF REPORT & PERIOD COVERED INTERIM REPORT Nov. 17, 1976-Nov. 1, 1977
		6. PERFORMING ORG. REPORT NUMBER (14) MR-7054
7. AUTHOR(s) (10) Harold S. Schechter, Martin O. Cohen		8. CONTRACT OR GRANT NUMBER(s) (15) DAAG39-77-C-0020 new
9. PERFORMING ORGANIZATION NAME AND ADDRESS MATHEMATICAL APPLICATIONS GROUP, INC. 3 Westchester Plaza Elmsford, N. Y. 10523		10. PROGRAM ELEMENT, PROJECT, TASK AREA & WORK UNIT NUMBERS (16) [redacted] 1L162118AH75 [redacted], PRON# A17R000402A1A9 (17) 00
11. CONTROLLING OFFICE NAME AND ADDRESS Harry Diamond Laboratories 2800 Powder Mill Road Adelphi, Md. 20783		12. REPORT DATE (11) Sep[redacted]977
		13. NUMBER OF PAGES (12) 64p.
14. MONITORING AGENCY NAME & ADDRESS (if different from Controlling Office)		15. SECURITY CLASS. (of this report) UNCLASSIFIED
		15a. DECLASSIFICATION/DOWNGRADING SCHEDULE

16. DISTRIBUTION STATEMENT (of this Report)

APPROVED FOR PUBLIC RELEASE; DISTRIBUTION UNLIMITED.

17. DISTRIBUTION STATEMENT (of the abstract entered in Block 20, if different from Report)

18. SUPPLEMENTARY NOTES

HDL Project No. X757E7

19. KEY WORDS (Continue on reverse side if necessary and identify by block number)

- Compton Electron Currents
- Energy Deposition
- Atmosphere
- Ground
- SAM-CE Monte Carlo Code
- Radial, Polar Components
- Time Dependence
- Neutron Source Energy Bands

20. ABSTRACT (Continue on reverse side if necessary and identify by block number)

A series of time-dependent Monte Carlo calculations has been performed to determine, as functions of neutron source energy band, the energy deposition rates and Compton electron sources in the air due to neutron and secondary photon interactions from weapons at 1-, 50-, 100-, and 200-m heights of burst. The calculations were made with a modified version of the SAM-CE computer program. → next page

DD FORM 1 JAN 73 1473 EDITION OF 1 NOV 65 IS OBSOLETE

UNCLASSIFIED

SECURITY CLASSIFICATION OF THIS PAGE (When Data Entered)

390 389

20.

The energy deposition rates and Compton electron sources were determined as functions of time (out to 100-ms local time), in 49 radial and altitude scoring bins surrounding the four isotropic point sources. Answers were obtained for penetrations from 0 to 2.4 km in the horizontal direction and from 0 to 1.5 km above the air-ground interface.

The raw data have been forwarded to HDL for smoothing and curve fitting. Sample results are presented and described in this report.

TABLE OF CONTENTS

LIST OF TABLES

LIST OF FIGURES

List of Tables (continued)

1. INTRODUCTION

Mathematical Applications Group, Inc. (MAGI) has performed a series of time-dependent Monte Carlo calculations to determine the energy-deposition rates and Compton electron sources in air due to neutron and secondary photon interactions from low-altitude nuclear bursts. These calculations were made with a modified version of the SAM-CE computer program.[1]

Isotropic sources of primary neutron radiation were considered at four low-altitude heights of burst (HOB); 1, 50, 100 and 200-m. Rather than treating specific weapon output energy spectra, as in previous work,[2] calculations were performed for contiguous neutron-source energy bands which, when combined, can reconstitute arbitrary neutron output spectra.

The energy deposition and Compton electron currents were determined as functions of time in 49 radial and altitude (R-Z) scoring bins surrounding a burst point. The atmosphere was taken to be homogeneous at an assumed density of 1.11 mg/cm^3. Answers were obtained for penetrations up to 2.4 km in the horizontal plane and up to 1.5 km above the ground.

---

1. M. O. Cohen et al., "SAM-CE: A Monte Carlo Code for Three Dimensional Neutron, Gamma Ray and Electron Transport (Revision 5)", MR-7052-5 (May 1977).

2. M. O. Cohen, H. S. Schechter, and H. A. Steinberg, "Time-Dependent Energy Deposition and Compton Electron Currents from Three Selected Low-Altitude Bursts", HDL-CR-76-029-1/MR-7048 (Aug. 1976).

2. COMPUTATIONAL TECHNIQUE

The calculations were performed with a specially modified version of the SAM-CE Monte Carlo program.[1] Alterations to the program, pertinent to the present calculations, include the following:

a. A special tracking procedure was used for neutrons with energies below the lowest inelastic threshold (for the nuclides which constitute the air and the ground). Also used was a special thermal diffusion model. These *ad hoc* procedures increased the computational efficiency by a factor of 5 to 10.

b. Time dependence was recorded in local time units defined as time subsequent to the arrival of the uncollided radiation. (For both primary neutron and secondary photon problems, local time zero is defined as the earliest possible arrival of photons.)

c. Time-dependent energy deposition due to neutron elastic scattering and photon Compton scattering was scored for all spatial regions.

d. Compton electron sources were scored in radial and polar bins. These are now described:

Figure 1 shows the basic source-detector geometry used in the Monte Carlo calculations.

A point isotropic source is located in the Cartesian coordinate system at $0,0,Z_s$, where Z_s is the source altitude, and a detector is located at X_d, Y_d, Z_d. The X and Y axes define a plane parallel to the ground.

Consider a vector score, $\overline{F}$, at the detector position. The score, in this case the average forward range of a Compton electron, can be characterized by its projections along the Cartesian X, Y, and Z axes. This is not the most convenient coordinate system, however. A more convenient coordinate system is defined by three mutually orthogonal vectors $\overline{1}_r$, $\overline{1}_p$, and $\overline{1}_\phi$ where $\overline{1}_r$ = the radial vector which is colinear to the source-detector axis; $\overline{1}_p$ = the polar vector, where $\overline{1}_r$ and $\overline{1}_p$ define a plane perpendicular to the ground; and $\overline{1}_\phi$ = the azimuthal vector, which is parallel to the ground.

(It is apparent that in a homogeneous atmosphere, the algebraic sum of all scores projected onto the azimuthal vector must vanish. Hence, in the Monte Carlo calculations, computer time was not spent projecting individual scores along this vector. The presence of the ground, however, does produce net scores along the polar axis, which would otherwise vanish in an infinite homogeneous air medium.)

---

1. M. O. Cohen *et al.*, "SAM-CE: A Monte Carlo Code for Three Dimensional Neutron, Gamma Ray and Electron Transport (Revision 5)", MR-7052-5 (May 1977).

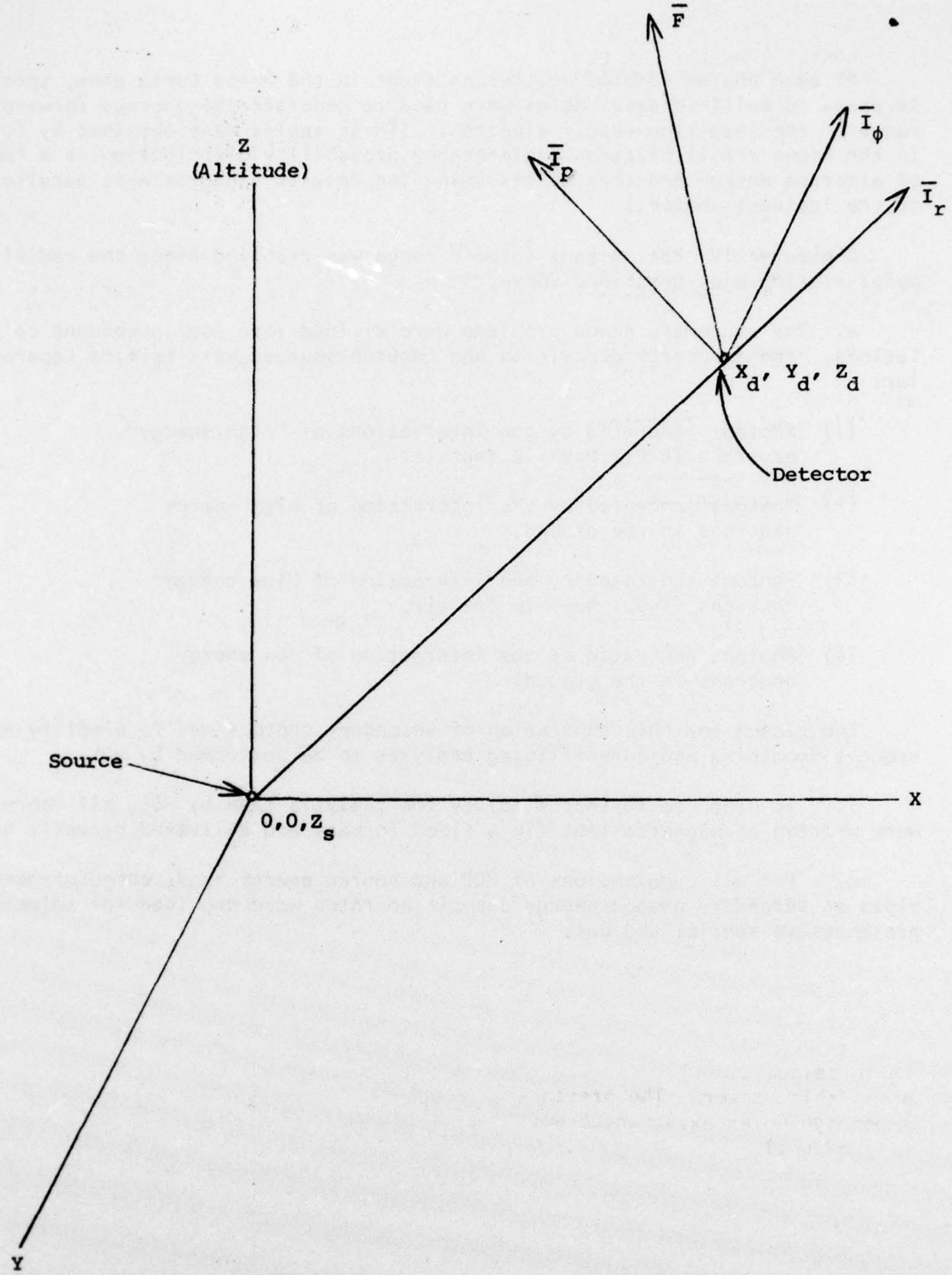

Figure 1 - Basic Source-Detector Geometry Used in the Monte Carlo Calculations

At each photon Compton scattering event in the Monte Carlo game, specially prepared built-in data tables were used to generate the average forward range of the resulting recoil electron. (These tables were obtained by folding in the known recoil electron angle-energy probability distribution as a function of electron energy and then by resolving the results along an axis parallel to the incident photon.)

Subsequently, the average forward range was resolved along the radial and polar scoring axes described above.

e. The secondary gamma problems were divided into four component calculations. Photon energy deposition and Compton sources were tallied separately for:

(1) Photons generated by the interactions of "high energy" neutrons (E>0.1 MeV) in the air.

(2) Photons generated by the interaction of high energy neutrons in the ground.

(3) Photons generated by the interaction of "low energy" neutrons (E<0.1 Mev) in the air.

(4) Photons generated by the interaction of low energy neutrons in the ground.

The reason for this separation of secondary photons was to simplify subsequent smoothing and curve-fitting analyses to be performed by HDL.

f. In order to further simplify the analysis task by HDL, all scores were written on magnetic tape (in a fixed format) and delivered directly to HDL.

g. For all combinations of HOB and source energy band, computer-generated plots of secondary photon energy deposition rates were provided for selected representative spatial regions.

3. CALCULATIONAL PROGRAM

3.1 Source Altitudes

Separate series of calculations were performed for HOB values of 1, 50, 100 and 200 meters.* The results obtained (see below) indicate that interpolation procedures will be adequate to scale the results to any other HOB in the ground-to-200 meter interval.

3.2 Source Energy Bands

The source energy band structure is given in Table 1. The 100m HOB problem was run first, and subsequent analyses of the sensitivity of the results to source energy showed that the final band structure (as used for the 1, 50, and 200m HOB runs) would be adequate.

3.3 Air and Ground Descriptions

The air composition, as used in the calculations, is given in Table 2. It represents dry air at a density of 1.11 mg/cm^3, corresponding to a height above sea level of approximately 900 m. A homogeneous model of the atmosphere was assumed.

The ground composition which was used is also given in Table 2. It corresponds to dry Nevada test soil at a density of 1.7 g/cm^3.

No attempts were made to assess the effects upon the results of moist air or ground compositions other than dry Nevada test soil.

3.4 Cross Sections and Response Functions

The cross section data base for the computations is given in Table 3. The average range data for Compton electrons, referred to in Section 2, were developed by the authors after consultation with various knowledgeable experts in the field.

3.5 Special Scoring Bins

The atmosphere was divided into stacked and concentric cylinders for the purposes of scoring and importance sampling (see Section 3.7). The spatial mesh was 300 m (33.3 g/cm^2). A finer subdivision of the atmosphere, however, was used closer to the source.

Figure 2 shows the spacing of the scoring regions and the identifying region number associated with each scoring bin. (The unlabeled regions were present in the monte Carlo calculations for backscattering purposes only.)

In order to investigate the behavior of the scored quantities near the air-ground interface, regions 2, 4, 10, and 12 were further subdivided as shown in Table 4.

*The 1 m HOB is used to represent a ground burst.

TABLE 1

Source Energy Band Structure

Band No.	Energy Interval (MeV)* 100m HOB	1, 50 and 200m HOB
1	0.0335 - 0.11	0.0335 - 0.11
2	0.11 - 0.55	0.11 - 0.55
3	0.55 - 1.11	0.55 - 1.11
4	1.11 - 1.83	1.11 - 1.83
5	1.83 - 2.35	1.83 - 2.35
6	2.35 - 3.01 **	2.35 - 4.07
7	3.01 - 4.07	4.07 - 6.36
8	4.07 - 4.97	6.36 - 8.19
9	4.97 - 6.36	8.19 -15.0
10	6.36 - 8.19	X
11	8.19 -10.00	X
12	10.00 -12.20	X
13	12.20 -15.00	X

*Uniform (i.e., flat) spectra are assumed within all bands.

**Brackets show multiple bands which were subsequently collapsed to a single band.

TABLE 2

Composition Descriptions

AIR (dry)

Photon Transport

N:	3.2501×10^{-2}	atom/g. air $\times 10^{24}$
O:	8.7201×10^{-3}	"
Aℓ:	1.9436×10^{-4}	"

Neutron Transport

N:	3.2655×10^{-2}	"
O:	8.7610×10^{-3}	"

GROUND (dry Nevada test soil)

Photon and Neutron Transport

H:	5.748×10^{-3}	atom/g. ground $\times 10^{24}$
O:	2.046×10^{-2}	"
Si:	6.822×10^{-3}	"
Aℓ:	2.872×10^{-3}	"

Density

Air: 1.11 mg/cm^3
Ground: 1.70 g/cm^3

TABLE 3

Cross Section Data Base

Element	Neutron Transport and Photon Production Data	Photon Transport Data
Hydrogen	DNA 4148-Mod 2	ENDF/B as disseminated by RSIC as Tape DLC-7 D.
Nitrogen	DNA 4133-Mod 4	
Oxygen	DNA4134-Mod 2	
Aluminum	DNA 4135-Mod 2	(all elements including Argon)
Silicon	DNA 4151-Mod 2	

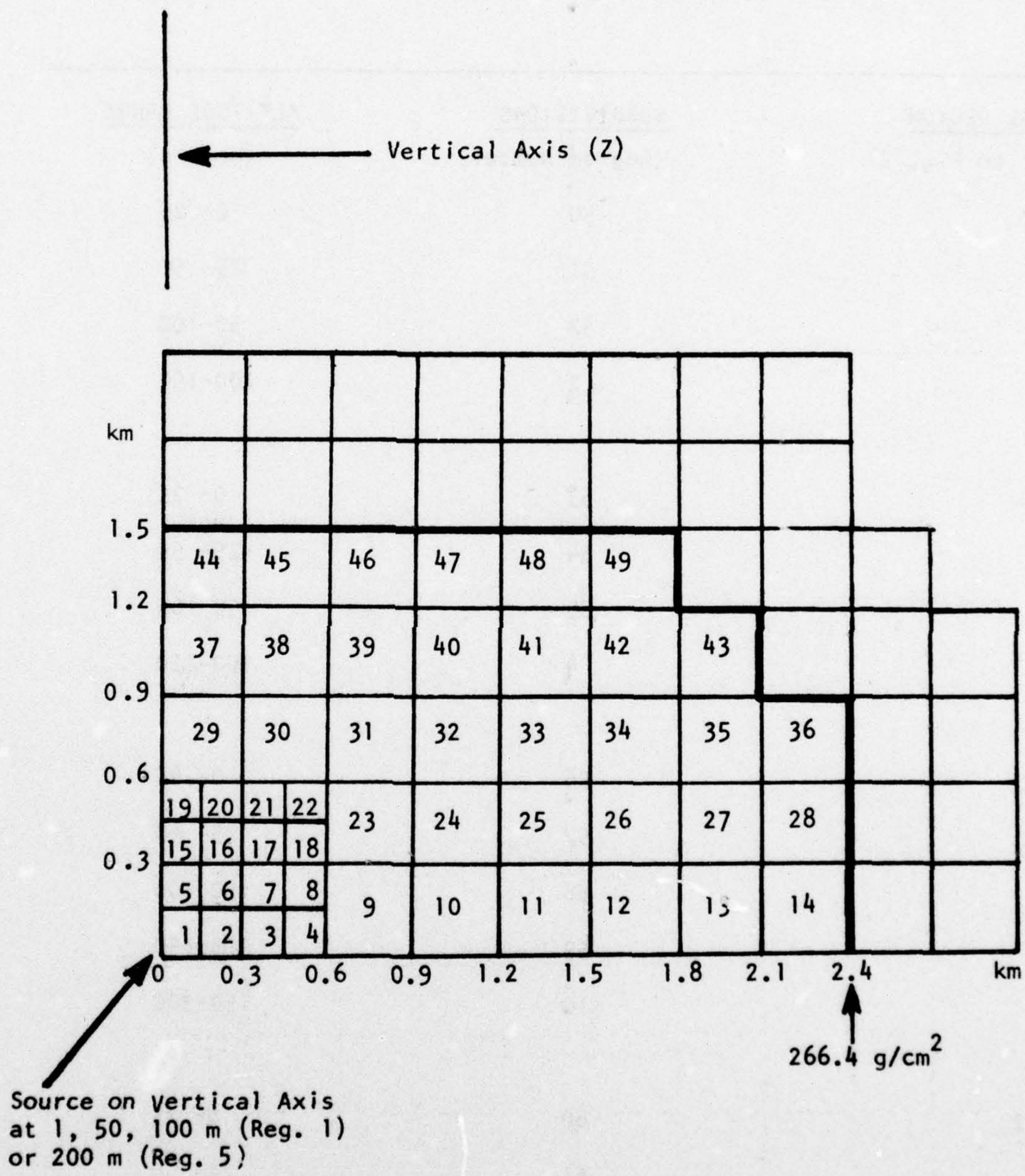

FIGURE 2 - Description of Scoring Regions

TABLE 4

Additional Subdivision of Selected Regions
Near the Air-Ground Interface

NOMINAL REGION (refer to Fig. 2)	SUBDIVISIONS (Region Number)	ALTITUDE RANGE (Meters)
2	50	0- 25
	51	25- 50
	52	50-100
	2	100-150
4	53	0- 25
	54	25- 50
	55	50-100
	4	100-150
10	56	0- 25
	57	25- 50
	58	50-100
	59	100-150
	10	150-300
12	60	0- 25
	61	25- 50
	62	50-100
	63	100-150
	12	150-300

3.6 Time Bins

The primary neutron and secondary photon scores were obtained in local time bins out to a 100 millisecond time cutoff. The local time structure is given in Table 5.

3.7 Importance Sampling

The problems to be solved involved difficult Monte Carlo importance sampling situations. Answers were required, with low statistical uncertainties, over many regions of a large multi-dimensioned phase space. Some of the techniques used to ensure adequate solutions included the following:

(a) Special tracking for neutrons below the inelastic threshold and a special thermal diffusion model - as described in Section 2, item (a).

(b) Energy importance sampling to discriminate against low energy neutron collisions which would be unlikely to generate secondary photons.

(c) Spatial importance sampling to generate a sufficient number of neutron high energy interactions at shallow penetrations (since the photons which they generate dominate the early temporal ranges).

(d) Spatial importance sampling to obtain adequate solutions at the deep penetrations and to "push" a sufficient number of neutron events towards the ground and towards the special subdivided volumes of Table 4.

(e) Directional importance sampling to discriminate against ground-generated photons initially headed downwards deeper into the ground.

TABLE 5

Time Bin Structure

Time Bin	Time Interval (sec)
1	(0 - 0.100) E-6
2	(0.100 - 0.215) E-6*
3	(0.215 - 0.464) E-6
4	(0.464 - 1.00) E-6
5	(1.00 - 2.15) E-6
6	(2.15 - 4.64) E-6
7	(4.64 - 10.0) E-6
8	(10.0 - 21.5) E-6
9	(21.5 - 46.4) E-6
10	(46.4 -100.0) E-6
11	(0.100 - 0.215) E-3
12	(0.215 - 0.464) E-3
13	(0.464 - 1.00) E-3
14	(1.00 - 2.15) E-3
15	(2.15 - 4.64) E-3
16	(4.64 - 10.0) E-3
17	(10.0 - 21.5) E-3
18	(21.5 - 46.4) E-3
19	(46.4 -100.0) E-3

*Read: 0.100×10^{-6} to 0.215×10^{-6} sec

4. DESCRIPTION OF RESULTS

4.1 Results Presented

The final results presented in this report will be sharply limited for the following reasons:

(a) The primary objective of the studies was to determine energy deposition rates and Compton current sources in the proscribed phase space bins and to forward these raw data to HDL for subsequent smoothing and curve-fitting analyses. This objective was met and results for each source band, at each HOB, have been delivered by MAGI to HDL as formatted output on magnetic tape.

(b) Much of the qualitative analyses for the previous study, involving fission and 14 MeV source,[1] apply to the band-source results of this study as well. These include:

(1) general temporal shapes of the neutron and four photon components of the energy deposition curves

(2) general temporal shapes of the four photon components of the radial and polar Compton current sources

(3) air-ground interface effects

(4) range and HOB effects on each of the above.

Hence, for such analyses, the reader is referred to the previous work. However, in the sections which follow, some of the salient new results are presented.

4.2 Variation of Time-Integrated Results by Source Band Energy

Table 6 displays the time-integrated energy deposition from the neutron and the four photon components in Region 32 (see Figure 2) as a function of source energy band. The results are for the 200-m HOB, integrated in time out to the 100 ms cutoff. Region 32 was selected for this first set of presented results because it is at an intermediate distance from the source, and is 600 to 900-m above the air-ground interface.

Table 6 shows that the high energy - air photon component is the most important contribution to the total dose for the higher energy source bands. However, as the neutron source energy drops below the air inelastic thresholds, this component completely disappears.

---

1. M. O. Cohen, H. S. Schechter, and H. A. Steinberg, "Time-Dependent Energy Deposition and Compton Electron Currents from Three Selected Low-Altitude Bursts", HDL-CR-76-029-1/MR-7048 (Aug. 1976).

TABLE 6

ENERGY DEPOSITION IN REGION 32

Weapon at 200-m HOB

(Integrated from local time 0 to 100 milliseconds)

Neutron Energy Band (MeV)	Component					Totals		
	Neutron	Photons						
		(High-energy air)	(High-energy ground)	(Low-energy air)	(Low-energy ground)	Photons Only	Neutrons Plus Photons	Neutron Fraction of Total Dose
.0335- .11	.42-17*			.29-11	.12-11	.41-11	.41-11	.00
.11 - .55	.54-14			.32-11	.17-11	.49-11	.49-11	.00
.55 - 1.11	.54-12			.47-11	.16-11	.63-11	.68-11	.08
1.11 - 1.83	.25-11			.60-11	.16-11	.76-11	.10-10	.25
1.83 - 2.35	.58-11		.25-13	.43-11	.19-11	.62-11	.12-10	.48
2.35 - 4.07	.98-11	.13-12	.41-13	.52-11	.15-11	.69-11	.17-10	.58
4.07 - 6.36	.14-10	.30-11	.15-12	.28-11	.12-11	.72-11	.21-10	.67
6.36 - 8.19	.20-10	.19-10	.41-12	.27-11	.12-11	.23-10	.43-10	.47
8.19 -15.0	.20-10	.44-10	.14-11	.33-11	.96-12	.50-10	.70-10	.29

*Read: 0.42×10^{-17} ev/(cm^3·source neutron)

The high energy - ground photon component is less important than the high energy - air component at the highest energies but extends down to lower neutron source energies due to the lower inelastic thresholds in the ground.

The two low-energy photon components are smaller than the high energy - air photon component at the highest neutron source energies. However, they remain markedly constant in their contribution (per source neutron) all the way down to the lowest neutron source band. In general, the total contribution from the low energy - air component is more than twice that of the low energy - ground. This would not have been our conclusion if the time cutoff had not been extended out to 100 ms, in contrast with the earlier work which was out to 10 ms.*

Table 6 also shows that neutron energy deposition is more than 50% of the total deposition in the neutron-source energy range of 2.35 to 6.36 MeV. Above 6.36 MeV, neutrons produce many high-energy air gamma rays, by inelastic scattering, which dominate the deposition of energy. Below 2.35 MeV the neutrons do not have much energy themselves but do produce capture gamma rays which dominate the deposition of energy. (The trends noted in this paragraph hold for all heights of burst and all spatial regions. For example, see Tables 7 through 11 which follow.)

Table 7 shows conditions similar to those of Table 6, except that the spatial region is 17, which is closer to the source (and to the ground) than is region 32. Similar trends are seen. It is noticed, however, that the low energy - ground component has been enhanced, vis-a-vis the low energy - air component and now exceeds the latter for some of the source energy bands. Also note that since the region is closer to the source, neutron-energy deposition dominates over a wider range of source energy bands.

Table 8 shows conditions for region 53 which is one of the subdivisions of region 4 (see Table 4) and which extends down to the ground. Trends similar to those noted above are again observable. Due to their nearness to the interface, both photon ground components have been enhanced vis-a-vis the photon air components. Indeed, the low energy - ground component clearly dominates the low energy - air component.

---

*For example, at the 100-m HOB an analysis of the low energy - air component for energy band no. 4 (~fission source) and band no. 13 (~14 Mev source) show 65% and 59%, respectively, of the time-integrated dose in the extra 10 to 100 ms time. By contrast, the values are 26% and 18%, respectively, for the low energy air - ground component.

TABLE 7

ENERGY DEPOSITION IN REGION 17

Weapon at 200-m HOB

(Integrated from local time 0 to 100 milliseconds)

Neutron Energy Band (MeV)	Component					Totals		
	Neutrons	Photons						
		(High-energy air)	(High-energy ground)	(Low-energy air)	(Low-energy ground)	Photons Only	Neutrons Plus Photons	Neutron Fraction of Total Dose
.0335- .11	.81-11*			.18-9	.53-10	.23-9	.24-9	.03
.11 - .55	.12-9			.17-9	.73-10	.24-9	.36-9	.33
.55 - 1.11	.39-9			.13-9	.74-10	.20-9	.59-9	.66
1.11 - 1.83	.78-9			.90-10	.49-10	.14-9	.92-9	.85
1.83 - 2.35	.10-8		.26-11	.64-10	.69-10	.14-9	.11-8	.91
2.35 - 4.07	.10-8	.51-11	.48-11	.48-10	.43-10	.10-9	.11-8	.91
4.07 - 6.36	.10-8	.19-9	.16-10	.26-10	.36-10	.27-9	.13-8	.77
6.36 - 8.19	.14-8	.86-9	.22-10	.36-10	.37-10	.96-9	.24-8	.58
8.19 -15.0	.12-8	.16-8	.48-10	.20-10	.31-10	.17-8	.29-8	.41

*Read: 0.81×10^{-11} ev/(cm^3·source neutron)

TABLE 8

ENERGY DEPOSITION IN REGION 53

Weapon at 200-m HOB

(Integrated from local time 0 to 100 milliseconds)

Neutron Energy Band (MeV)	Component					Totals		
	Neutrons	Photons						
		(High-energy air)	(High-energy ground)	(Low-energy air)	(Low-energy ground)	Photons Only	Neutrons Plus Photons	Neutron Fraction of Total Dose
.0335- .11	.26-12*			.83-10	.54-10	.14-9	.14-9	.00
.11 - .55	.14-10			.58-10	.74-10	.13-9	.14-9	.10
.55 - 1.11	.81-10			.62-10	.20-9	.26-9	.34-9	.24
1.11 - 1.83	.17-9			.56-10	.15-9	.21-9	.38-9	.45
1.83 - 2.35	.25-9		.14-11	.56-10	.17-9	.23-9	.48-9	.52
2.35 - 4.07	.28-9	.11-11	.12-10	.39-10	.10-9	.15-9	.43-9	.65
4.07 - 6.36	.44-9	.64-10	.29-10	.21-10	.99-10	.20-9	.64-9	.69
6.36 - 8.19	.44-9	.33-9	.51-10	.24-10	.67-10	.47-9	.91-9	.48
8.19 -15.0	.33-9	.60-9	.92-10	.24-10	.56-10	.77-9	.11-8	.30

*Read: 0.26×10^{-12} ev/(cm^3·source neutron)

TABLE 9

ENERGY DEPOSITION IN REGION 32

Weapon at 1-m HOB

(Integrated from local time 0 to 100 milliseconds)

Neutron Energy Band (MeV)	Component					Totals		
	Neutrons	Photons						
		(High-energy air)	(High-energy ground)	(Low-energy air)	(Low-energy ground)	Photons Only	Neutrons Plus Photons	Neutron Fraction of Total Dose
.0335- .11	.14-18*			.14-11	.29-11	.43-11	.43-11	.00
.11 - .55	.14-14			.21-11	.38-11	.59-11	.59-11	.00
.55 - 1.11	.93-13			.25-11	.31-11	.56-11	.57-11	.02
1.11 - 1.83	.83-12			.28-11	.27-11	.55-11	.63-11	.13
1.83 - 2.35	.21-11		.18-12	.36-11	.25-11	.63-11	.84-11	.25
2.35 - 4.07	.40-11	.83-14	.33-12	.22-11	.20-11	.45-11	.85-11	.47
4.07 - 6.36	.74-11	.18-11	.17-11	.20-11	.22-11	.77-11	.15-10	.49
6.36 - 8.19	.94-11	.91-11	.35-11	.18-11	.16-11	.16-10	.25-10	.38
8.19 -15.0	.89-11	.23-10	.89-11	.18-11	.19-11	.36-10	.45-10	.20

*Read: 0.14×10^{-18} ev/(cm^3·source neutron)

TABLE 10

ENERGY DEPOSITION IN REGION 17

Weapon at 1-m HOB

(Integrated from local time 0 to 100 milliseconds)

Neutron Energy Band (MeV)	Component					Totals		
	Neutrons	Photons						
		(High-energy air)	(High-energy ground)	(Low-energy air)	(Low-energy ground)	Photons Only	Neutrons Plus Photons	Neutron Fraction of Total Dose
.0335- .11	.82-12*			.61-10	.16-9	.22-9	.22-9	.00
.11 - .55	.18-10			.74-10	.16-9	.23-9	.25-9	.07
.55 - 1.11	.13-9			.99-10	.14-9	.24-9	.37-9	.35
1.11 - 1.83	.28-9			.71-10	.12-9	.19-9	.47-9	.60
1.83 - 2.35	.40-9		.21-10	.62-10	.14-9	.22-9	.62-9	.65
2.35 - 4.07	.49-9	.24-11	.59-10	.38-10	.10-9	.20-9	.69-9	.71
4.07 - 6.36	.53-9	.81-10	.10-9	.33-10	.82-10	.30-9	.83-9	.64
6.36 - 8.19	.59-9	.37-9	.21-9	.28-10	.78-10	.69-9	.13-8	.45
8.19 -15.0	.56-9	.69-9	.43-9	.27-10	.83-10	.12-8	.18-8	.31

*Read: 0.82×10^{-12} ev/(cm^3·source neutron)

TABLE 11

ENERGY DEPOSITION IN REGION 53

Weapon at 1-m HOB

(Integrated from local time 0 to 100 milliseconds)

Neutron Energy Band (Mev)	Component					Totals		
	Neutrons	Photons						
		(High-energy air)	(High-energy ground)	(Low-energy air)	(Low-energy ground)	Photons Only	Neutrons Plus Photons	Neutron Fraction of Total Dose
.0335- .11	.23-12*			.38-10	.31-10	.69-10	.69-10	.00
.11 - .55	.57-11			.44-10	.55-10	.99-10	.10-9	.06
.55 - 1.11	.46-10			.56-10	.67-10	.12-9	.17-9	.27
1.11 - 1.83	.12-9			.60-10	.99-10	.16-9	.28-9	.43
1.83 - 2.35	.20-9		.48-11	.54-10	.90-10	.15-9	.35-9	.57
2.35 - 4.07	.20-9	.13-11	.12-10	.35-10	.13-9	.18-9	.38-9	.53
4.07 - 6.36	.26-9	.49-10	.36-10	.29-10	.58-10	.17-9	.43-9	.60
6.36 - 8.19	.39-9	.20-9	.43-10	.27-10	.67-10	.34-9	.73-9	.53
8.19 -15.0	.28-9	.39-9	.74-10	.23-10	.59-10	.55-9	.83-9	.34

*Read: 0.23×10^{-12} ev/(cm^3·source neutron)

TABLE 12

GAMMA RAY ENERGY DEPOSITION; RATIO OF 1-m HOB to 200-m HOB

ENERGY BAND (MeV)	COMPONENT: High Energy-Air Region 17	32	53	High Energy-Ground Region 17	32	53	Low Energy-Air Region 17	32	53	Low Energy-Ground Region 17	32	53
.0335- .11							0.3	0.5	0.5	3.0	2.4	0.6
.11 - .55							0.4	0.7	0.8	2.2	2.2	0.7
.55 - 1.11							0.8	0.5	0.9	1.9	1.9	0.3
1.11 - 1.83							0.8	0.5	1.1	2.4	1.7	0.7
1.83 - 2.35				8.1	7.2	3.4	1.0	0.8	1.0	2.0	1.3	0.5
2.35 - 4.07	0.5	0.1	1.2	13.4	8.0	1.0	0.8	0.4	0.9	2.3	1.3	1.3
4.07 - 6.36	0.4	0.6	0.8	6.3	11.3	1.2	1.3	0.7	1.4	2.3	1.8	0.6
6.36 - 8.19	0.5	0.5	0.6	9.5	8.5	0.8	0.8	0.7	1.1	2.1	1.3	1.0
8.19 -15.0	0.4	0.5	0.7	9.0	6.4	0.8	1.4	0.5	1.0	2.7	2.0	1.1

Tables 9, 10 and 11 are repeats of Tables 6, 7 and 8, except that the height of burst has been lowered from 200-m to 1-m. For regions 17 and 32, the ground-photon component is seen to be greatly enhanced. (Also see Table 12, below). For region 53, the line-of-sight from the source to the detector for the 1-m case is so close to the horizontal that the ground component may actually be decreased in some cases (also see Table 12, which follows) vis-a-vis the 200-m HOB case.

Table 12 displays the ratio of the gamma ray deposition components for the 1-m and 200-m heights of burst. For regions 17 and 32, it is seen that lowering the source height from 200-m to 1-m:

(a) reduces the high energy - air component by about one-half,

(b) greatly enhances the high energy - ground component by about a factor of ten,

(c) reduces somewhat (sometimes less than by one-half) the low energy - air component, and

(d) enhances the low energy - ground component by about a factor of 2 which is a smaller enhancement than for the high energy - ground component.

Region 53 is an exception, as explained in the preceding paragraph. The results for a 1-m HOB and a 200-m HOB are much closer to each other than was the case for regions 17 and 32.

4.3 Time-Dependent Results

Figures 3 through 34, which follow, display representative energy deposition rates in regions 1, 17, 32, and 53 for the 50-m height of burst. (Region 1 contains the source.) Trends similar to those of the 50-m HOB were found for the other three altitudes.

In all figures, the ordinate values are in units of eV/(cm^3·sec·source neutron), and the abscissa values are in units of seconds (of local time)*. Except for the neutron deposition histograms, the symbols on the plots represent the calculational statistical accuracy to the nearest tens of percent. For example, a "3" represents 30% statistics. For neutrons, where only zeros (0) appear, statistics are not available.

Figures 3 through 22 display the results for the 4.07 through 6.36 MeV range which is representative of the higher neutron source energies.

Figures 3 through 6 show the neutron results, for this source energy band, for regions 1, 17, 32, and 53, respectively. Figure 3, for region 1, shows the energy deposition existing as local time goes to zero. This is to be expected, since region 1 contains the source. Between 10^{-6} and 10^{-5} seconds the pulse begins a rapid decay with time and disappears, for all practical purposes, by 10^{-3}

---

*Recall that local time zero is defined as the earliest possible time of arrival of secondary gamma radiation.

seconds. Figures 4-6 show the arrival of the neutron pulse at $\sim 10^{-5}$ seconds and then similar decay schemes. In fact, the pulse shapes of Figure 3-6 are qualitatively similar to the corresponding curves for other heights-of-burst, spatial regions, and source bands.

Figures 7-10 show the low energy-air results for regions 1, 17, 32 and 53, respectively. Although slight variations exist, these curves are representative of the results found for all heights-of-burst, spatial regions and source bands. The curves rise steeply at about 10^{-3} seconds, may show a slight rise for a short time period, (e.g., see Figure 8) and then decay away rather slowly in time out to the cutoff of this problem which is 10^{-1} seconds.

Figures 11-14 show the results for the same four spatial regions for the low-energy ground component. Neutrons slow down much more rapidly in the ground than in the air and thus they are also captured more quickly. Hence, the low-energy ground component arrives at 10^{-6} to 10^{-5} seconds, the exact value depending upon the HOB and the altitude of the detector region. Also note that by the cutoff time of 10^{-1} seconds, the magnitude of this component has been reduced from the peak value by several orders of magnitude. The decay of the low energy - ground component, as shown in Figures 11-14, is characteristic of all heights-of-burst, spatial regions, and source energies.

Figures 15-18 display the high energy-air component for the four spatial regions. Since neutrons can collide at time zero (0) and produce high energy gamma rays which fly uncollided out to a scoring region, this component of the energy deposition is seen to exist at the earliest local times. After remaining relatively constant for several orders of magnitude of local time (for which theoretical arguments, not given here, can be provided) this component decays away rapidly and vanishes at about 10^{-5} to 10^{-4} seconds. The shape of these figures is characteristic for all heights of burst and all spatial regions. However, they are very much a function of source band energy. Indeed, the component does not even exist below the inelastic threshold in air (e.g., see Table 6).

Figures 19-22 display the high energy - ground component for the four spatial regions. The shape of the pulse is characteristic of all heights of burst and spatial regions, but, as was the case for the high energy - ground component, a function of the source and energy. Note that the pulse is of relatively short duration, rising at about 10^{-6} seconds (thus being a function of the HOB, i.e., the flight distance from source to the ground) and decaying away by about 10^{-4} seconds.

Figures 23-34 are for 0.55-1.11 MeV, which is one of the low-energy source bands. They correspond to Figures 3-14, respectively, for the 4.07-6.36 Mev band. There are no corresponding figures to Figures 15-22 since, as noted above, the high energy photon components do not exist for this source energy band.

Comparisons of Figures 23-34 with the corresponding Figures 3-14 bear out the comments made above that the characteristic shapes of the neutron and low energy photon components are relatively independent of neutron source energy band.

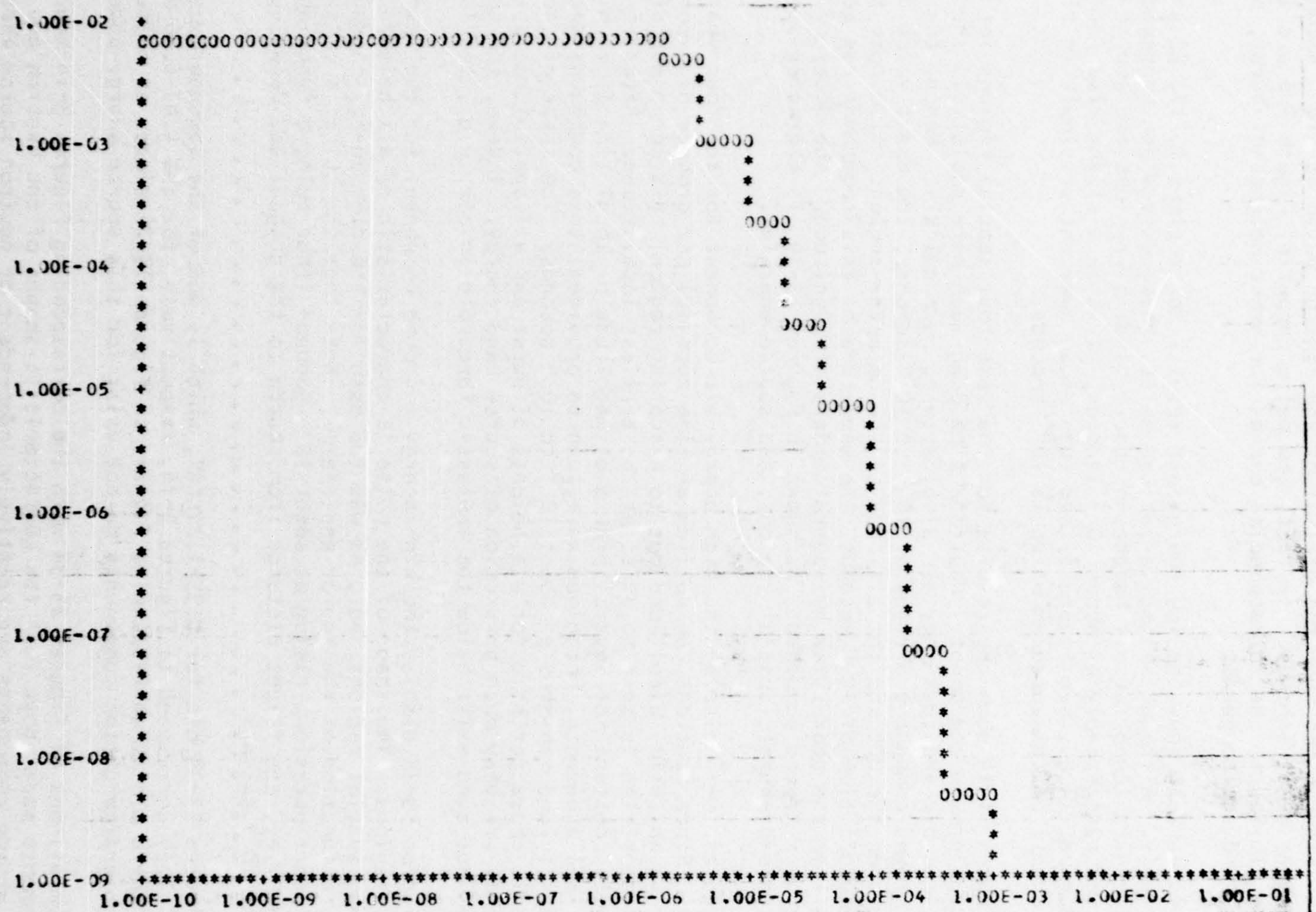

HDL3 50 M 6.36-4.07 MEV NEUTRONS

FIGURE 3 REGION 1 INTEGRAL= 0.4147E-07

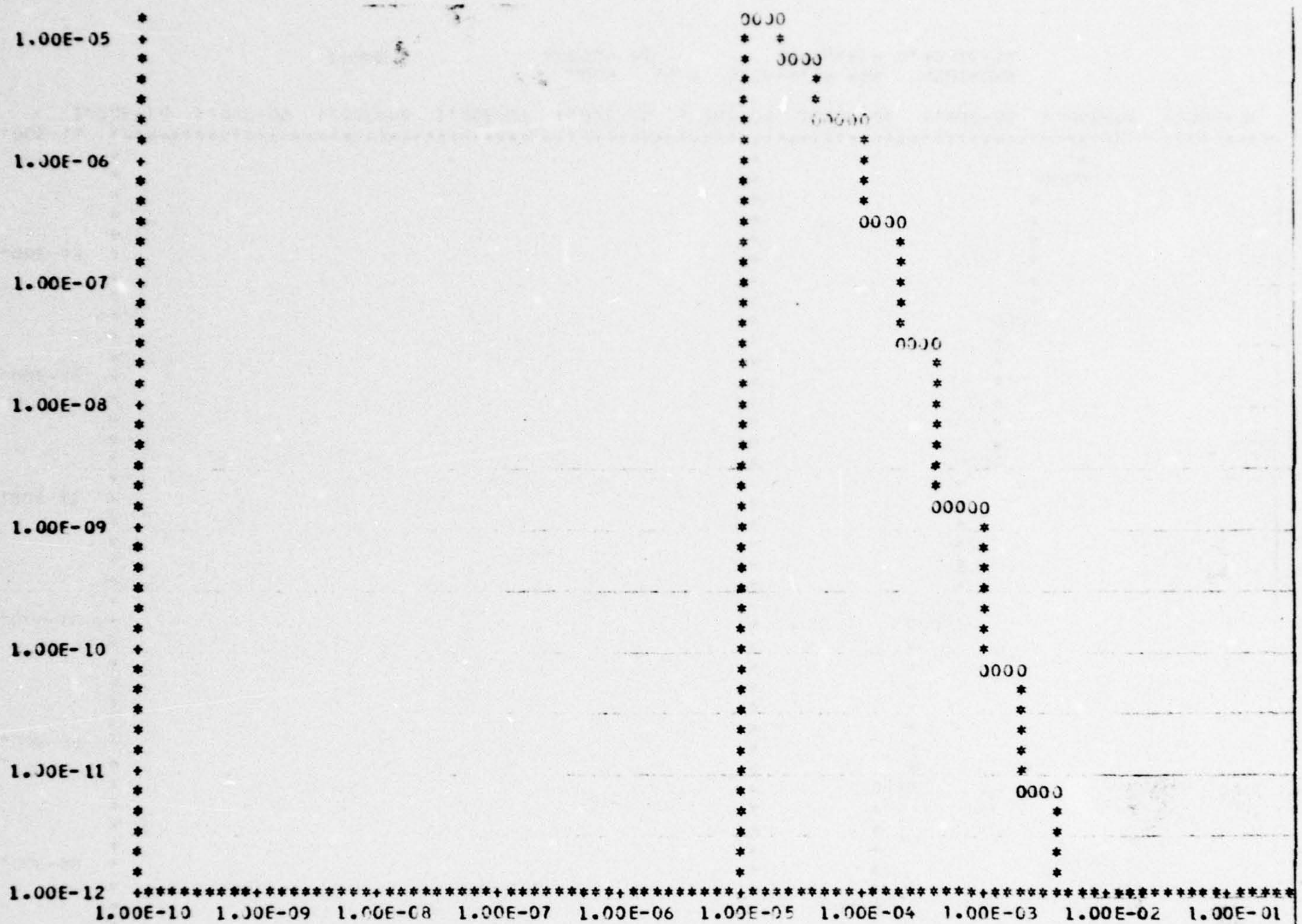

HDL3 50 M 6.36-4.07 MEV NEUTRONS
REGION 17 INTEGRAL= 0.6232E-09

FIGURE 4

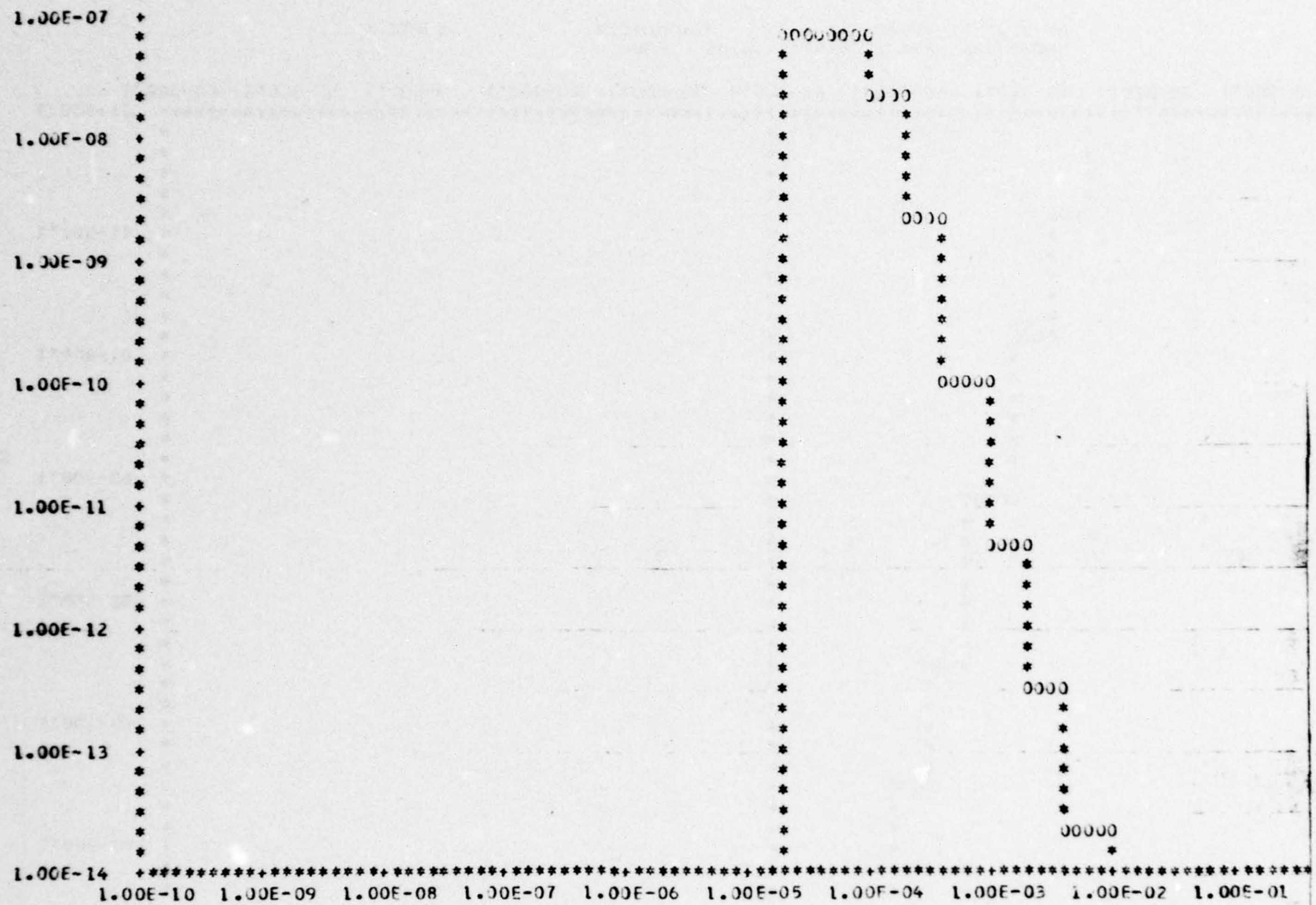

FIGURE 5

HDL3 50 M 6.36-4.07 MEV NEUTRONS
REGION 32 INTEGRAL = 0.9231E-11

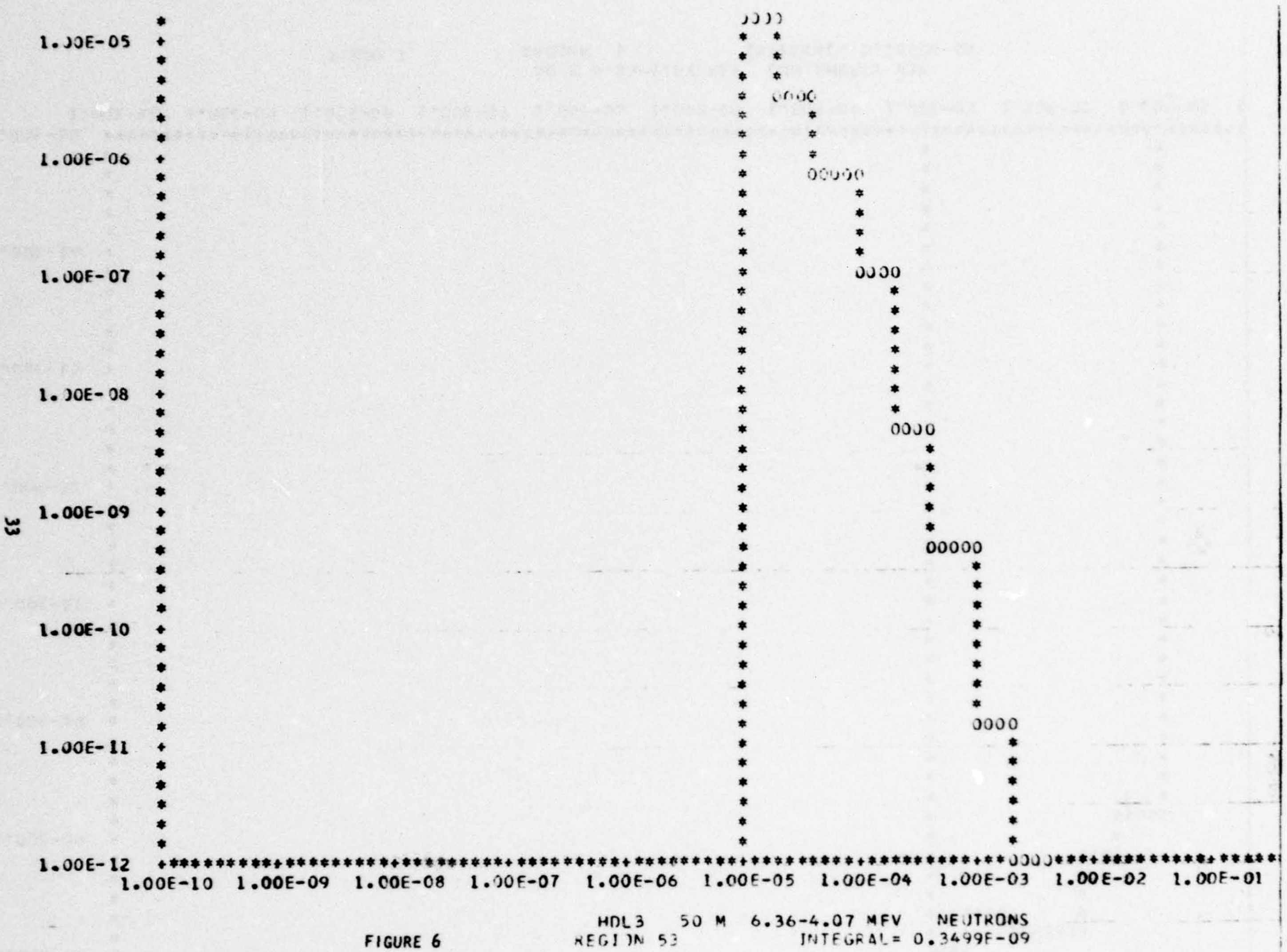
1.00E-05
1.00E-06
1.00E-07
1.00E-08
1.00E-09
1.00E-10
1.00E-11
1.00E-12
1.00E-10 1.00E-09 1.00E-08 1.00E-07 1.00E-06 1.00E-05 1.00E-04 1.00E-03 1.00E-02 1.00E-01
HDL3 50 M 6.36-4.07 MEV NEUTRONS
REGION 53 INTEGRAL= 0.3499E-09

FIGURE 6

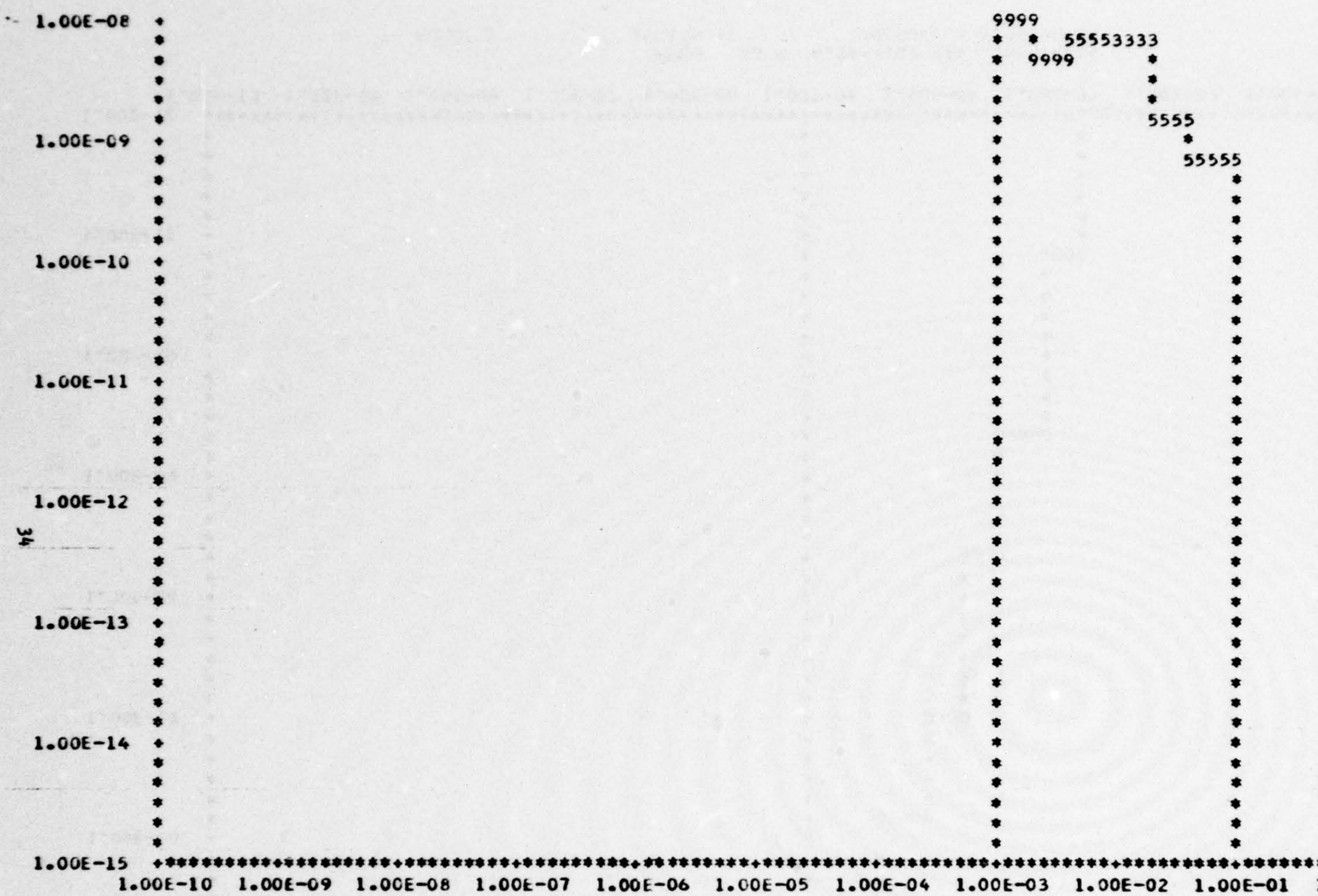

50 M 6.36-4.07 MEV LOW ENERGY AIR

FIGURE 7 REGION 1 INTEGRAL= 0.2560E-09

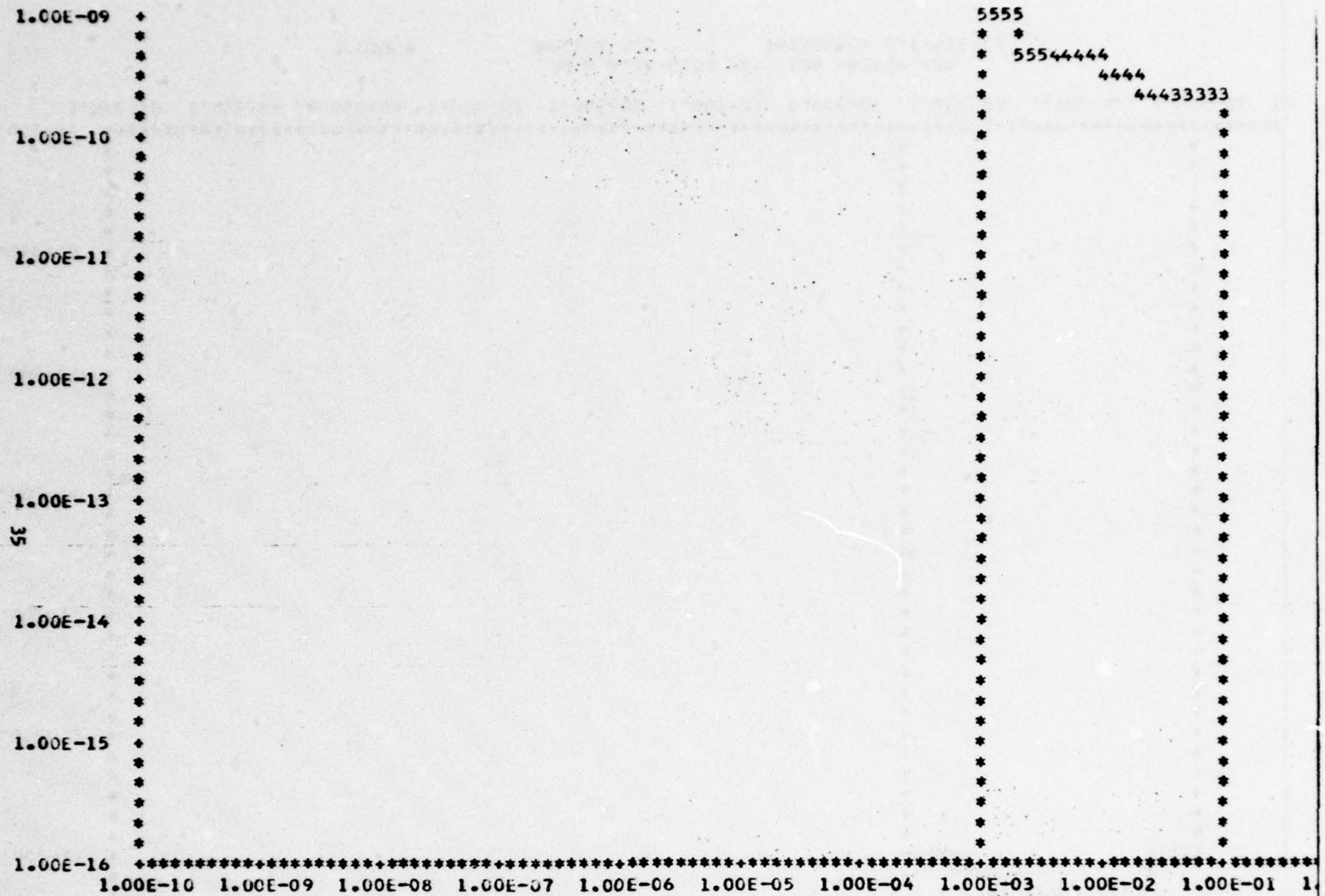

FIGURE 8

50 M 6.36-4.07 MEV LOW ENERGY AIR
REGION 17 INTEGRAL= 0.3356E-10

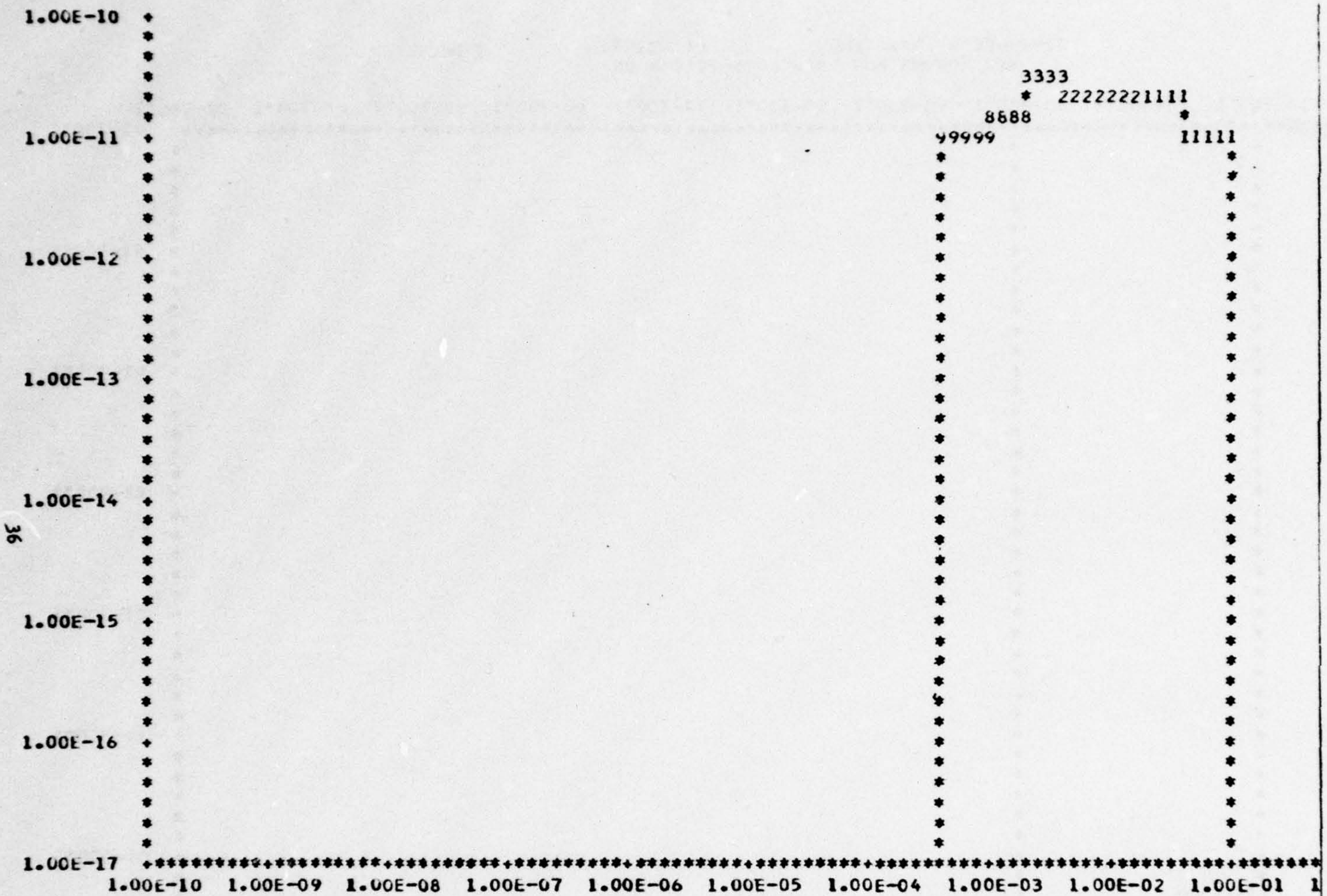

50 M 6.36-4.07 MEV LOW ENERGY AIR

FIGURE 9 REGION 32 INTEGRAL= 0.1952E-11

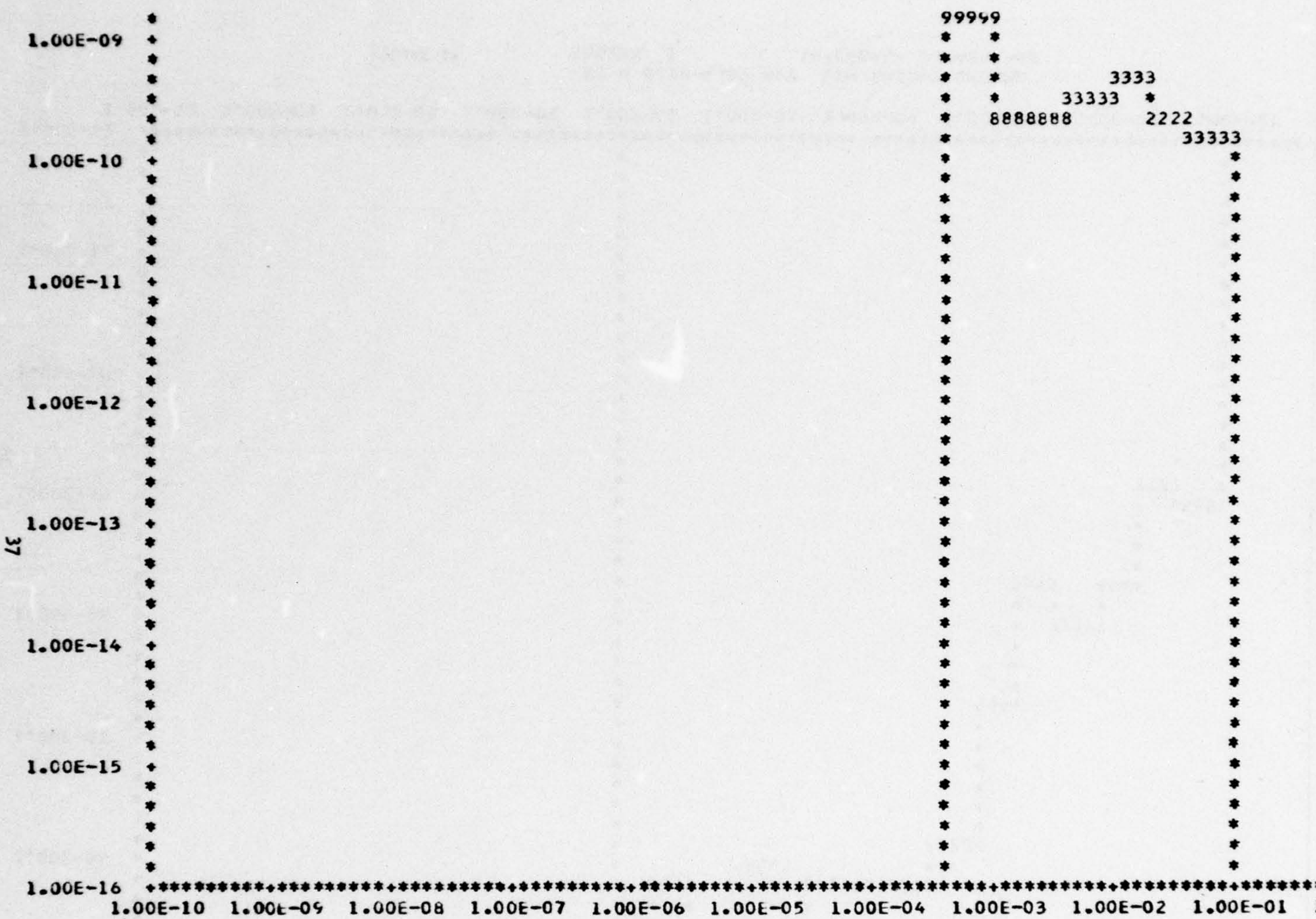

50 M 6.36-4.07 MEV LOW ENERGY AIR

FIGURE 10 REGION 53 INTEGRAL= 0.2656E-10

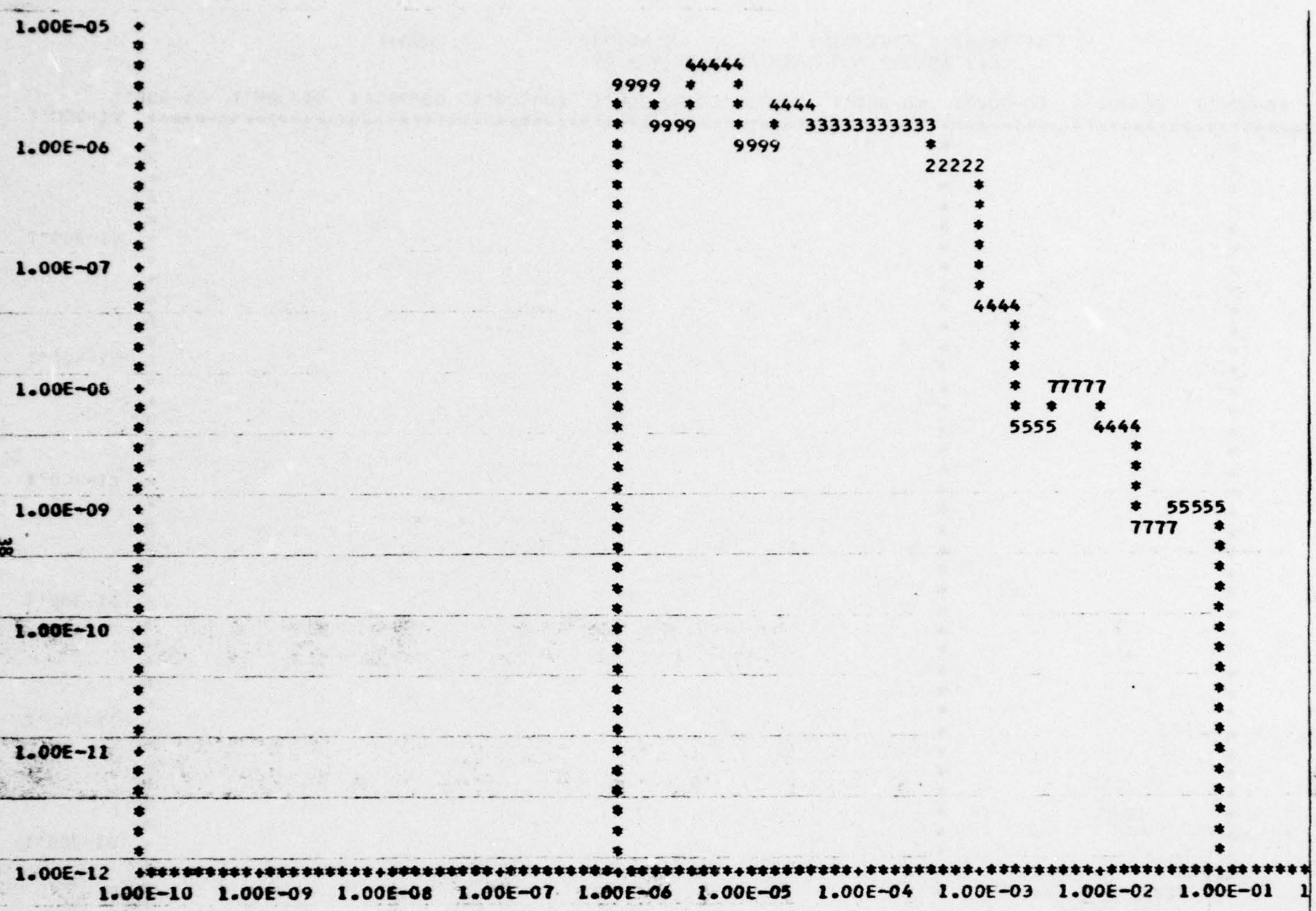

FIGURE 11

50 M 6.36-4.07 MEV LOW ENERGY GROUND
REGION 1 INTEGRAL= 0.1486E-08

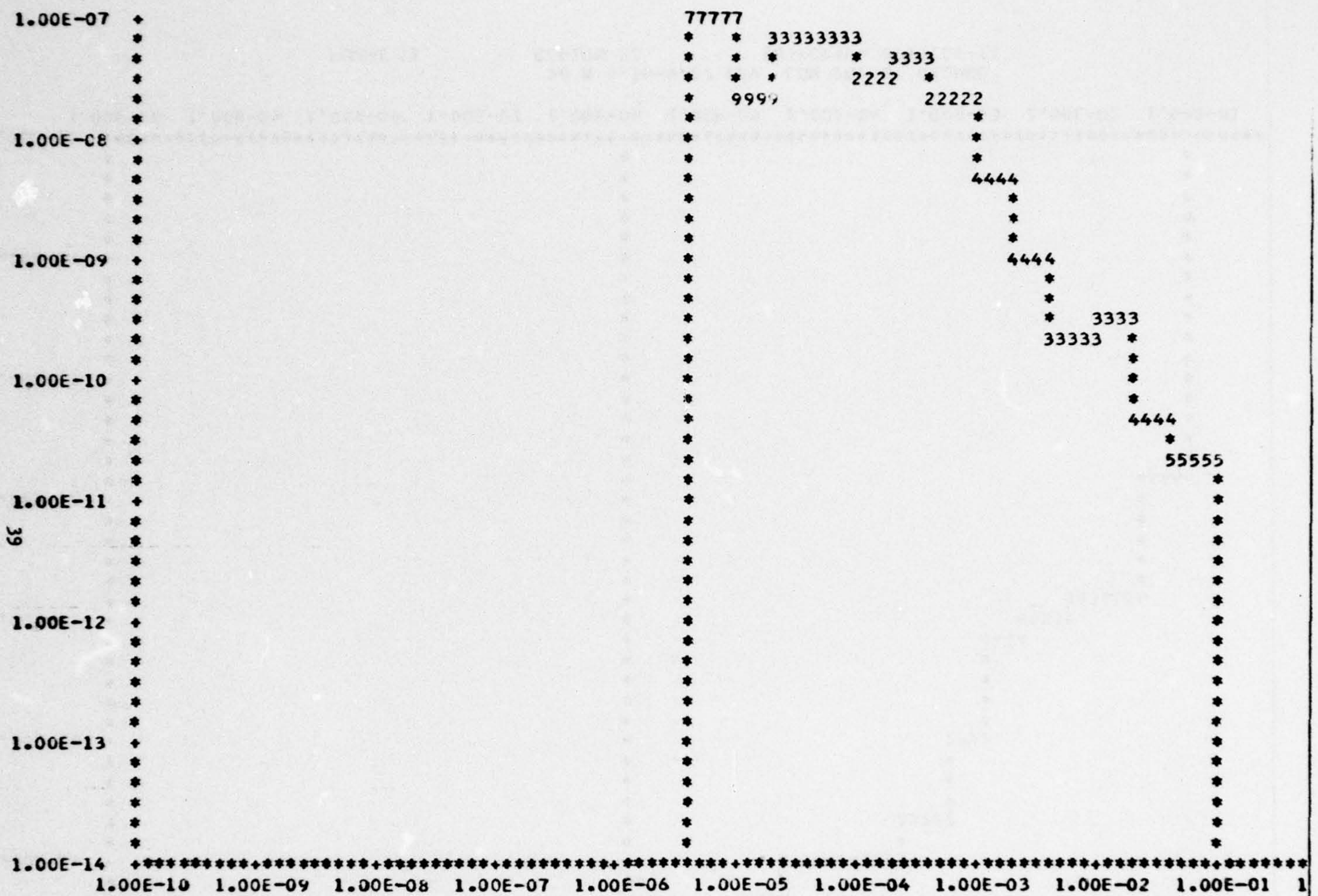

50 M 6.36-4.07 MEV LOW ENERGY GROUND

FIGURE 12 REGION 17 INTEGRAL= 0.5714E-10

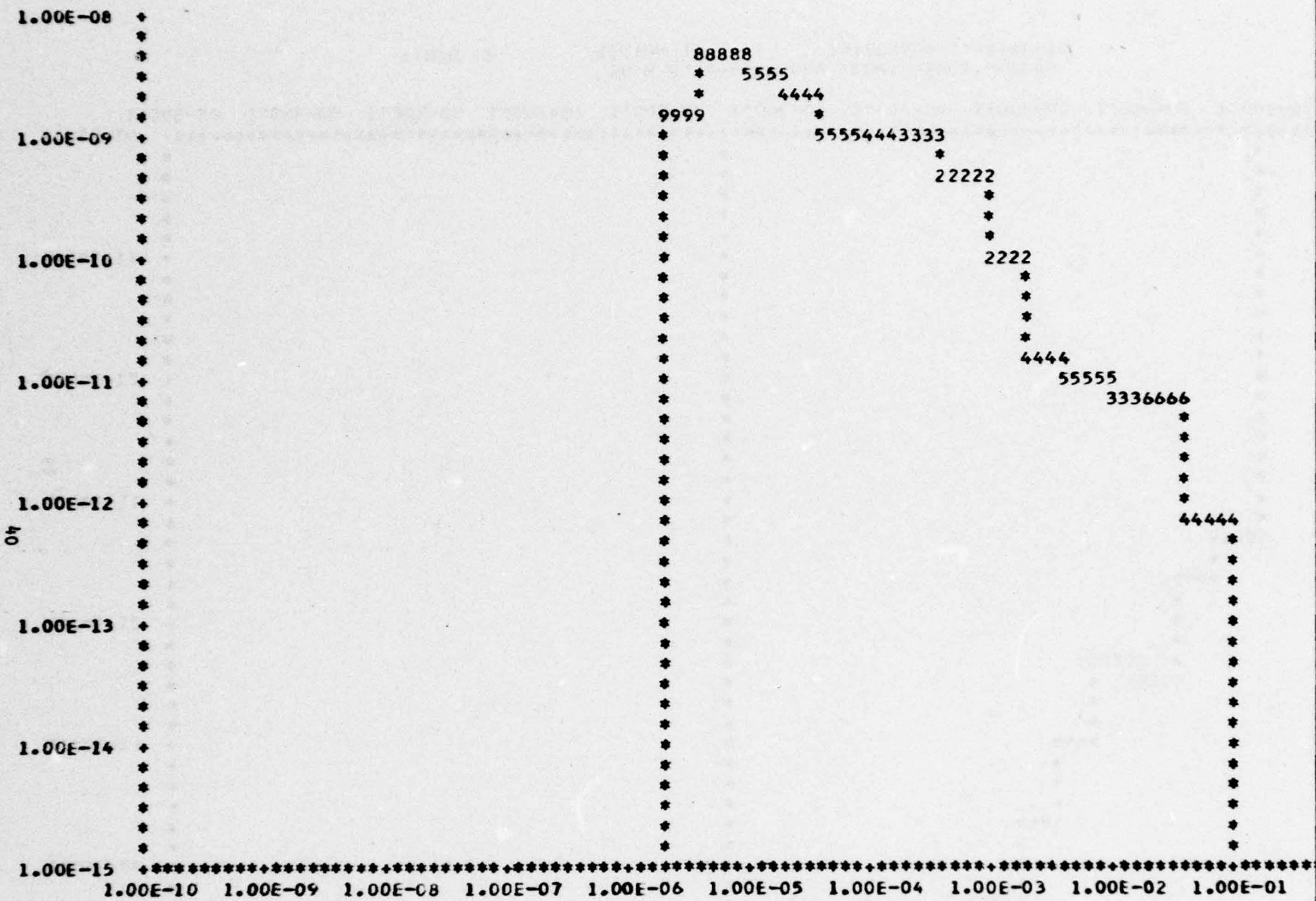

50 M 6.36-4.07 MEV LOW ENERGY GROUND

FIGURE 13 REGION 32 INTEGRAL= 0.1510E-11

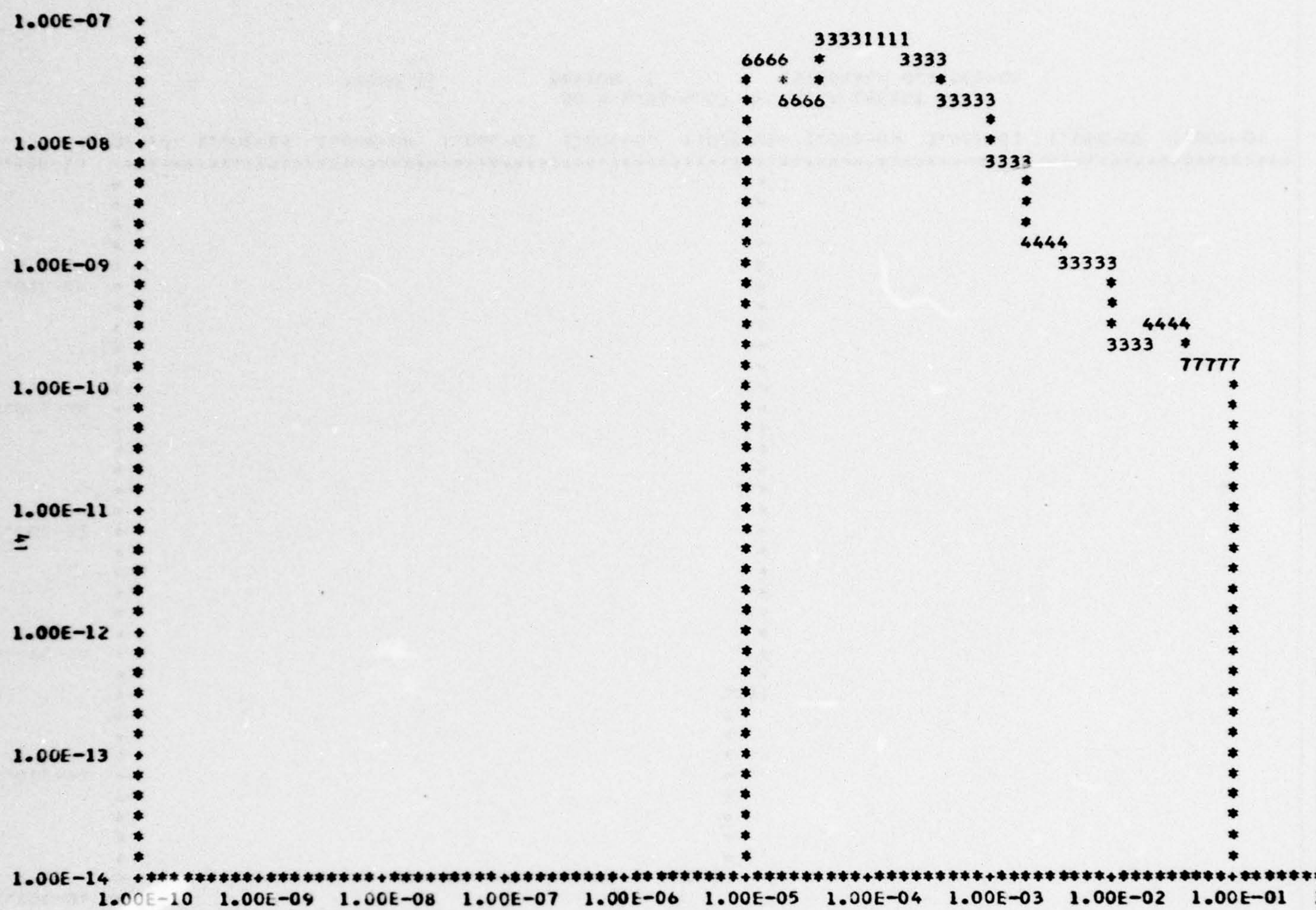

FIGURE 14

50 M 6.36-4.07 MEV LOW ENERGY GROUND
REGION 53 INTEGRAL= 0.9414E-10

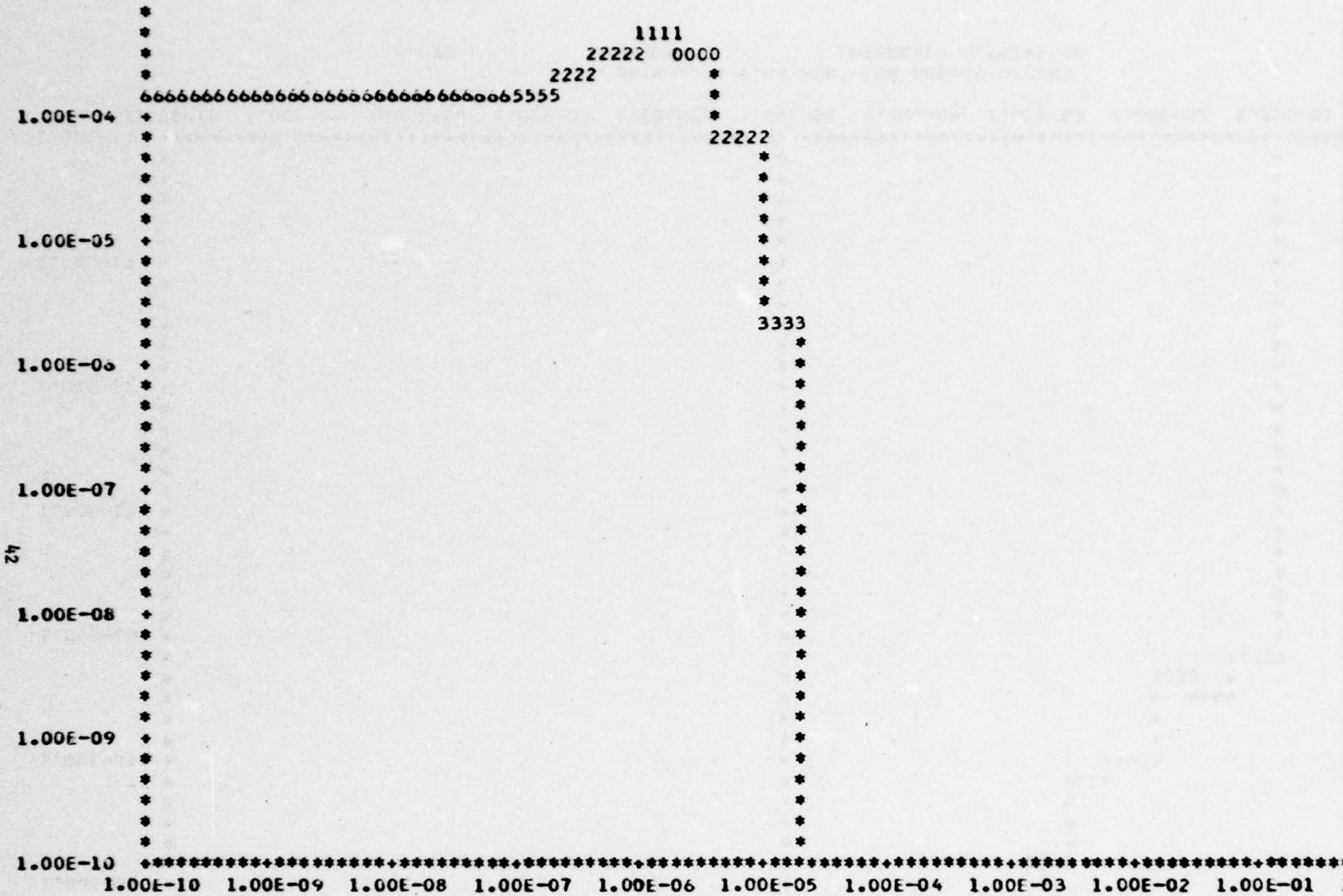

50 M 6.36-4.07 MEV HIGH ENERGY AIR

FIGURE 15 REGION 1 INTEGRAL= 0.2150E-08

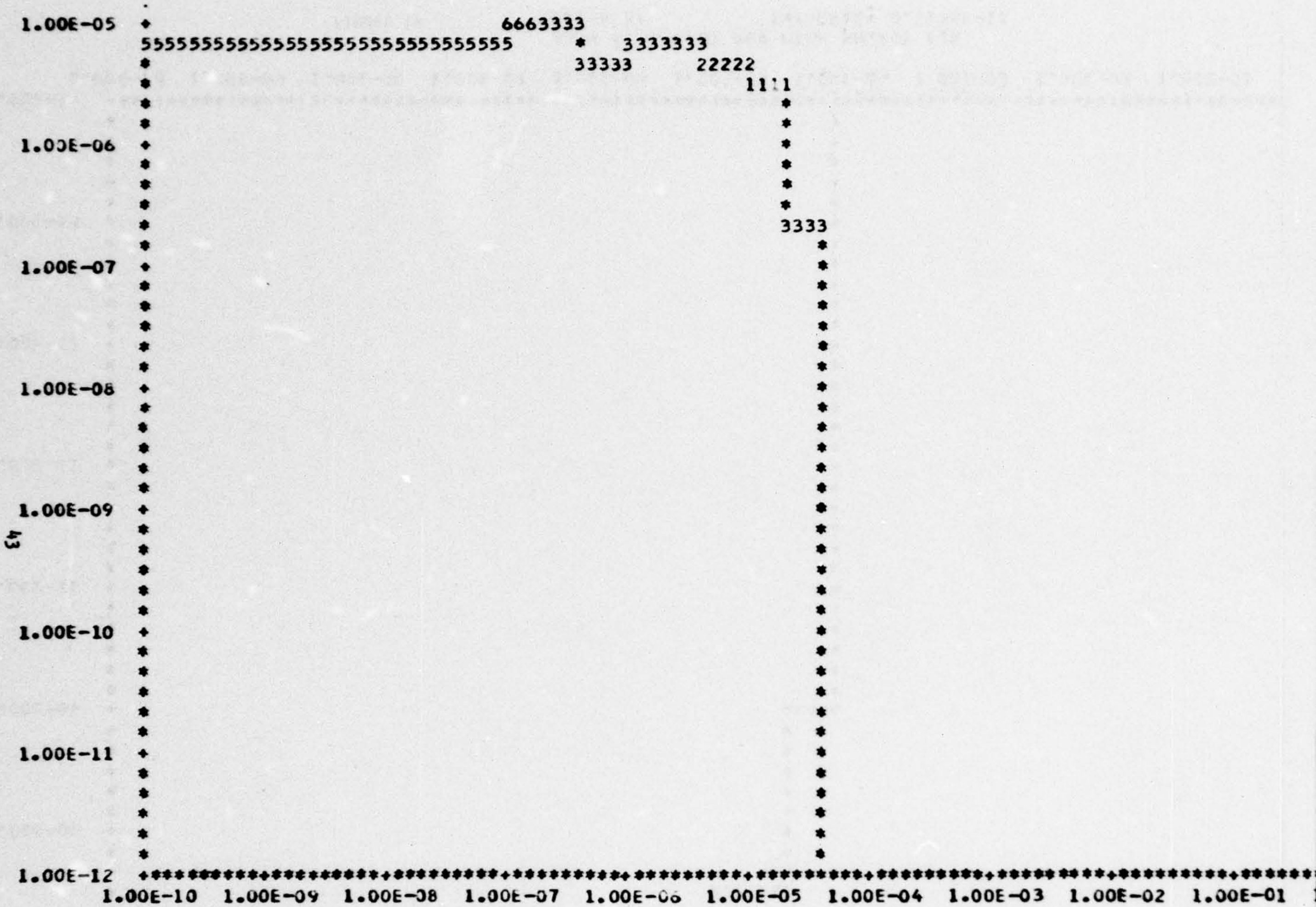

50 M 6.36-4.07 MEV HIGH ENERGY AIR

REGION 17 INTEGRAL= 0.1205E-09

FIGURE 16

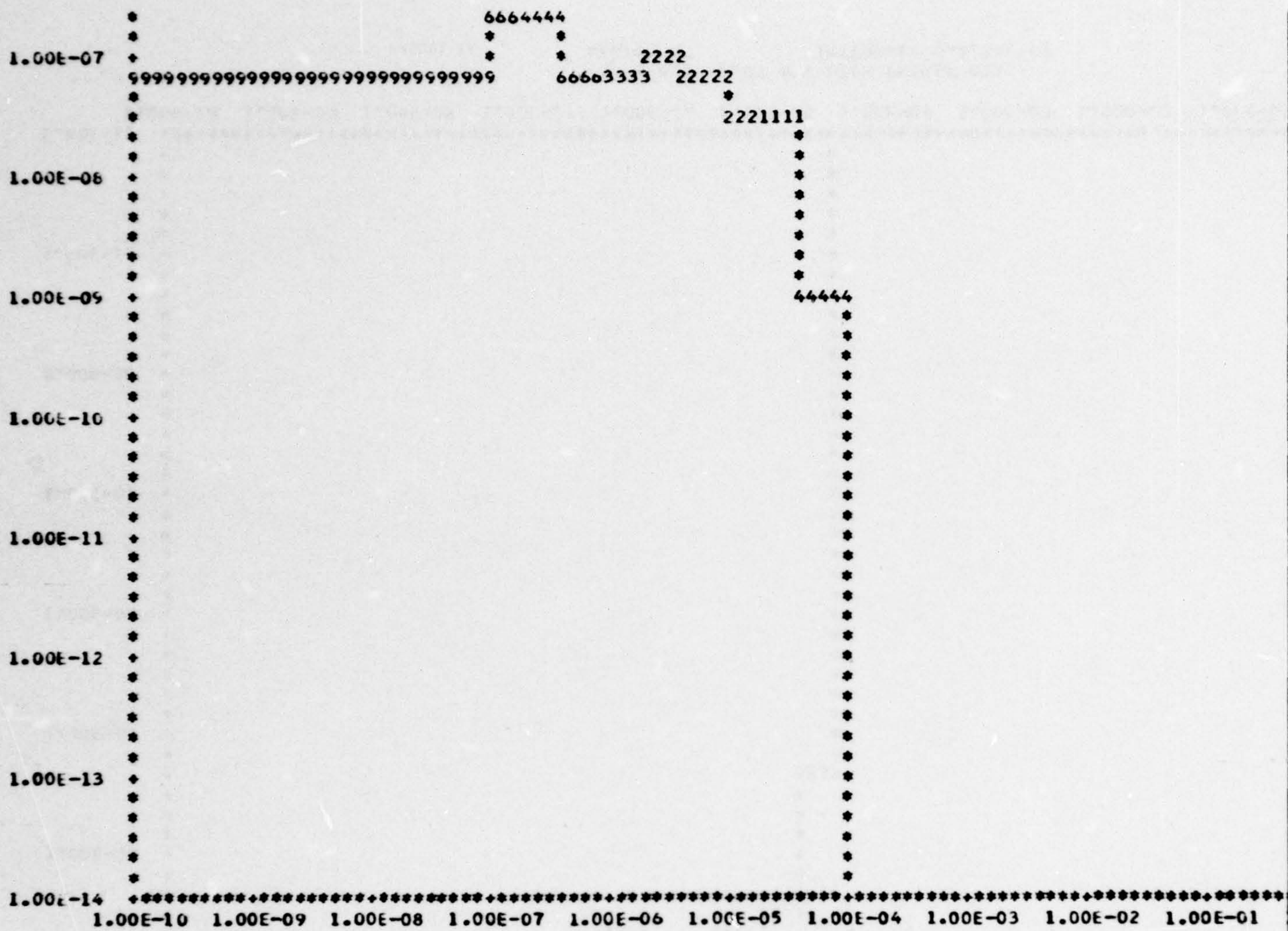

FIGURE 17

5G M 6.36-4.07 MEV HIGH ENERGY AIR
REGION 32 INTEGRAL= 0.2186E-11

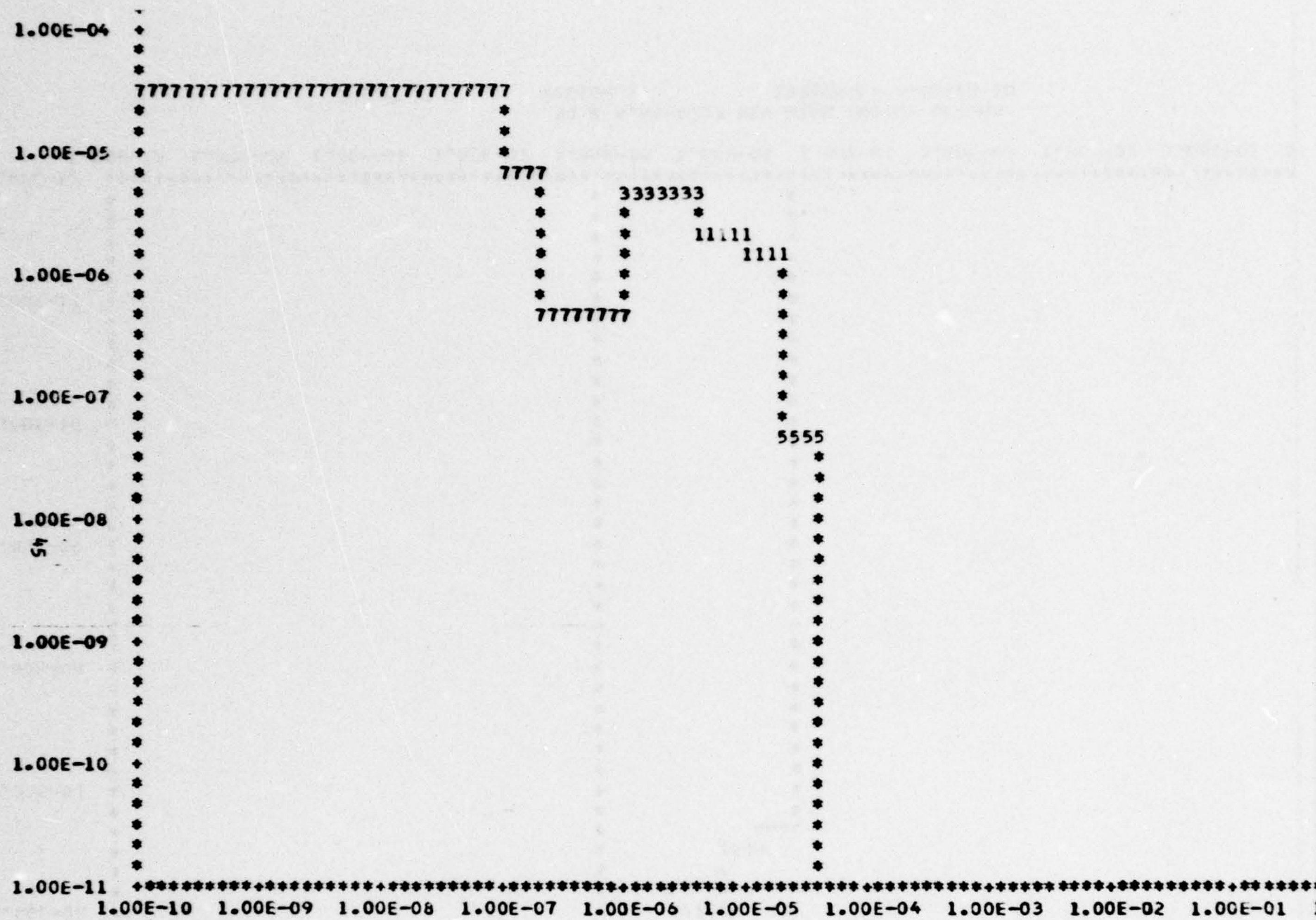

50 M 6.36-4.07 MEV HIGH ENERGY AIR

FIGURE 18 REGION 53 INTEGRAL= 0.6312E-10

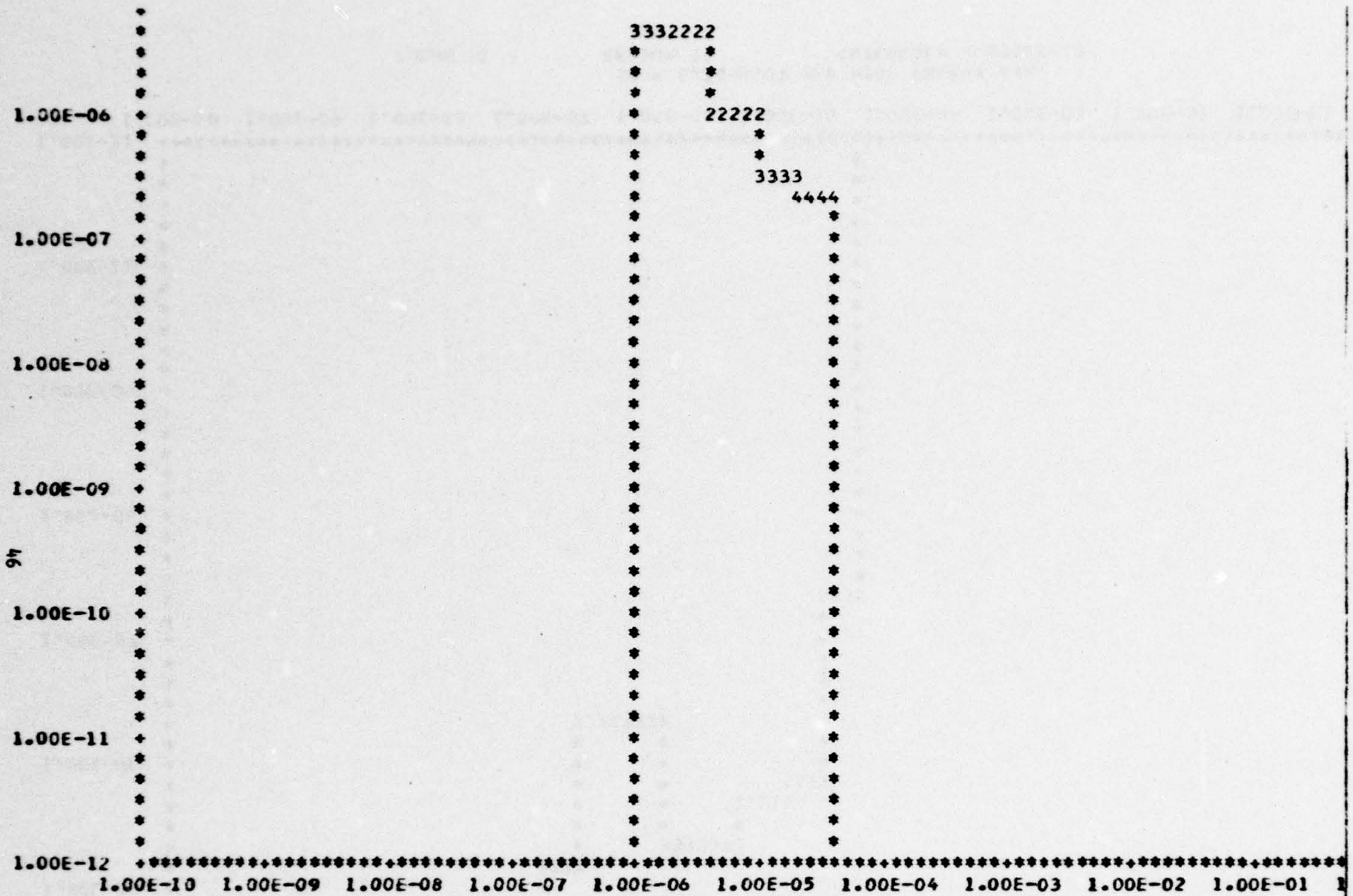

50 M 6.36–4.07 MEV HIGH ENERGY GROUND

FIGURE 19 REGION 17 INTEGRAL= 0.4082E-10

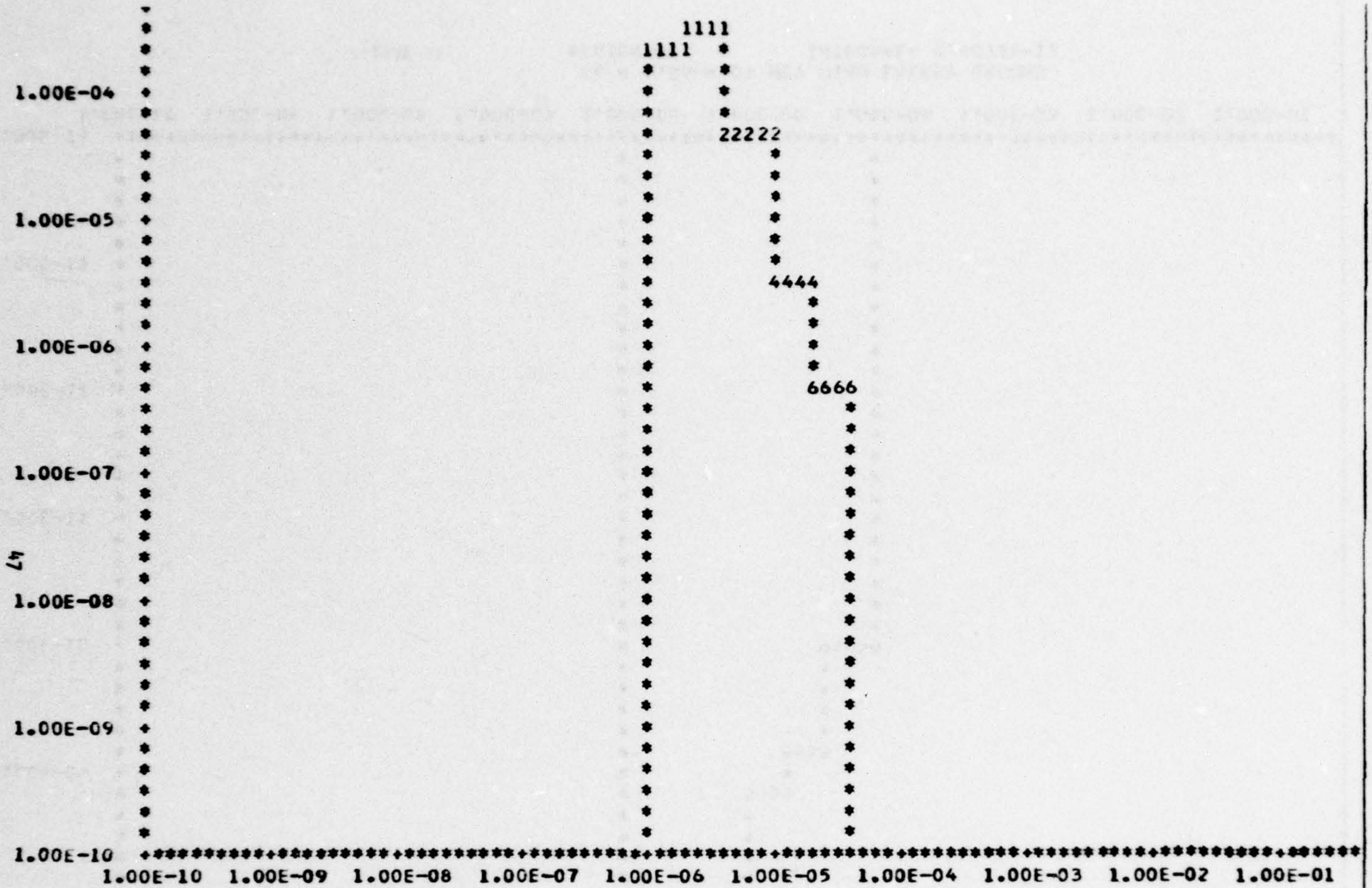

FIGURE 20

50 M 6.36-4.07 MEV HIGH ENERGY GROUND

REGION 1

INTEGRAL= 0.1654E-08

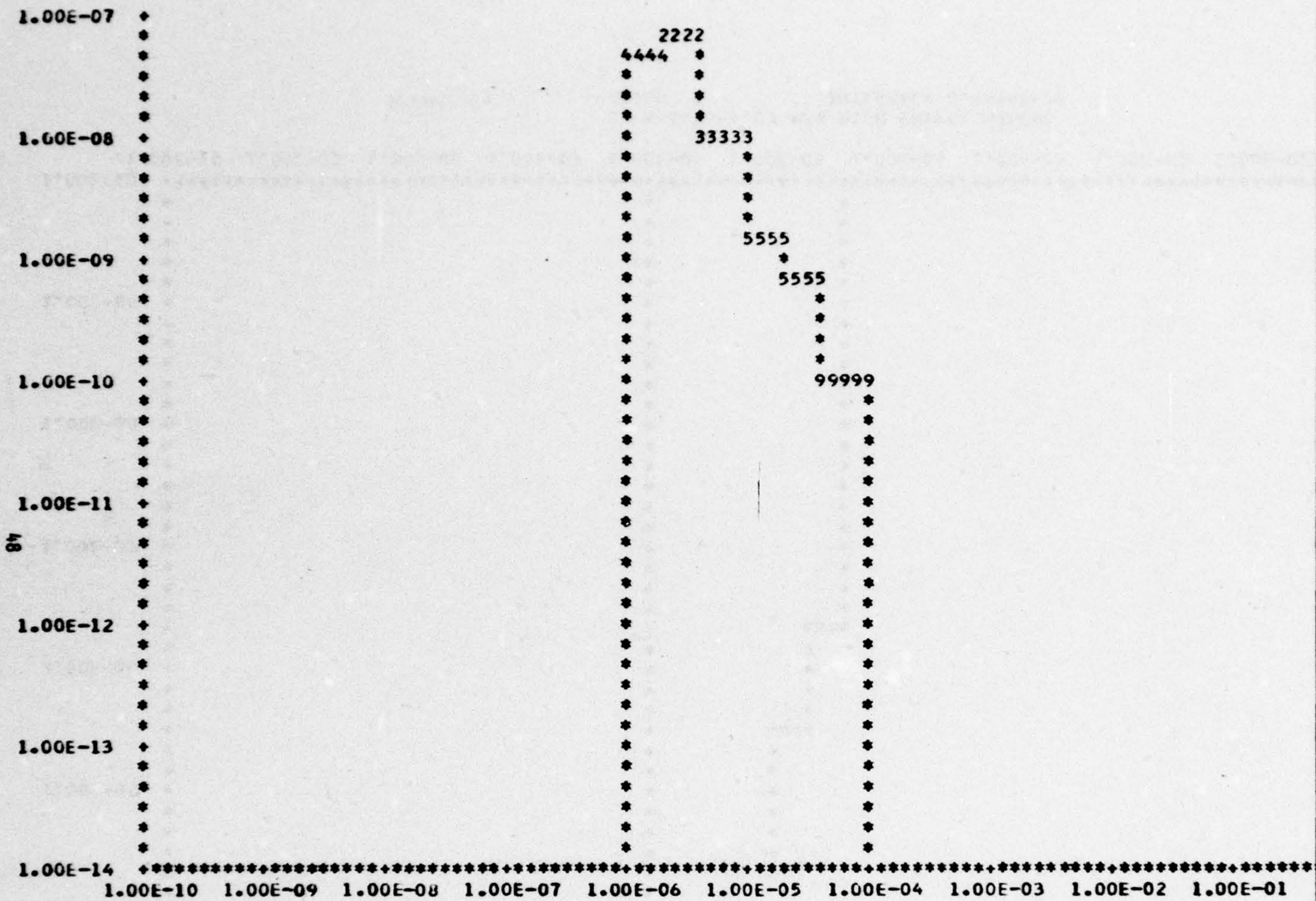

50 M 6.36-4.07 MEV HIGH ENERGY GROUND

FIGURE 21 REGION 32 INTEGRAL= 0.4073E-12

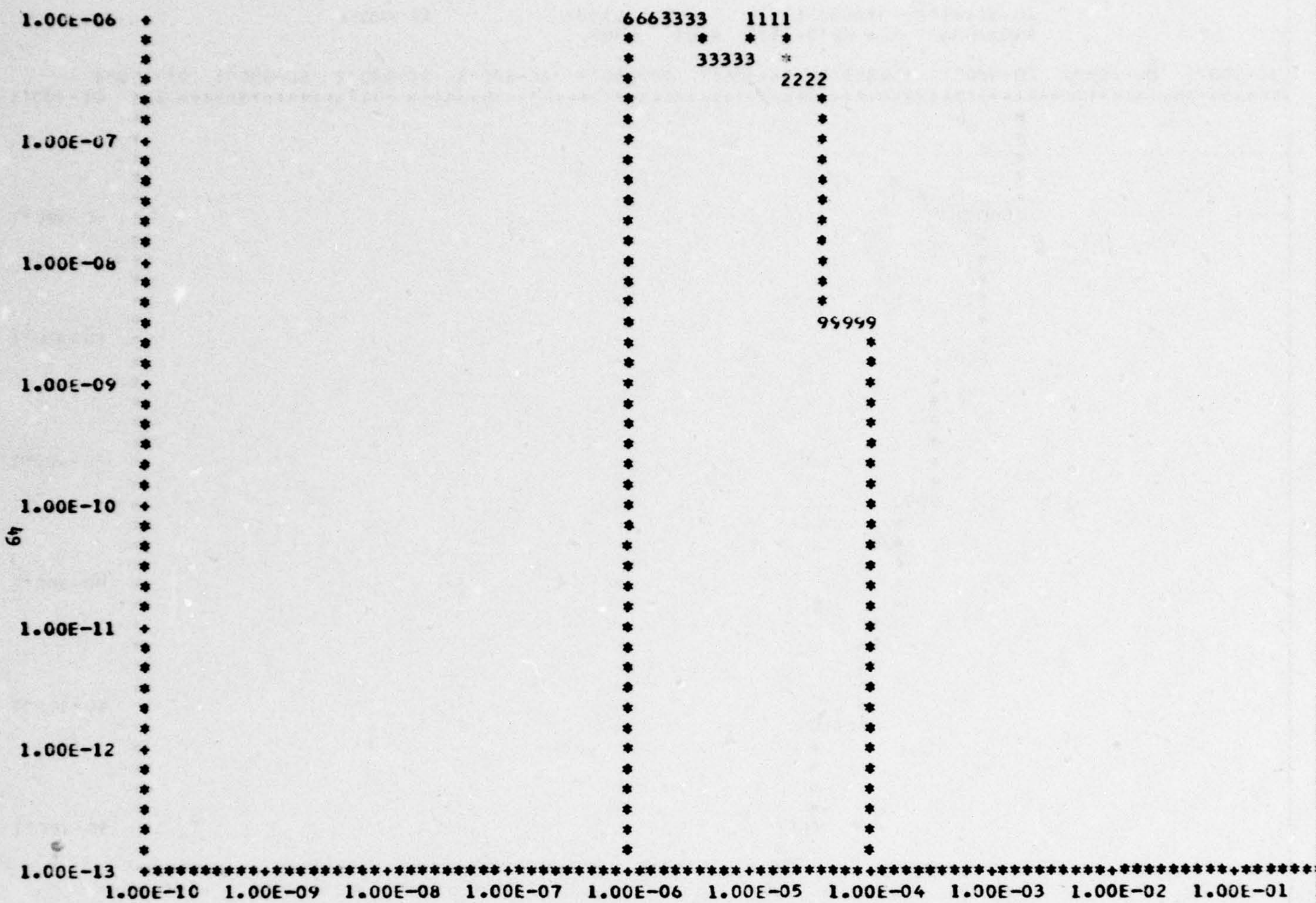

FIGURE 22

50 M 6.36-4.07 MEV HIGH ENERGY GROUND
REGION 53 INTEGRAL= 0.2958E-10

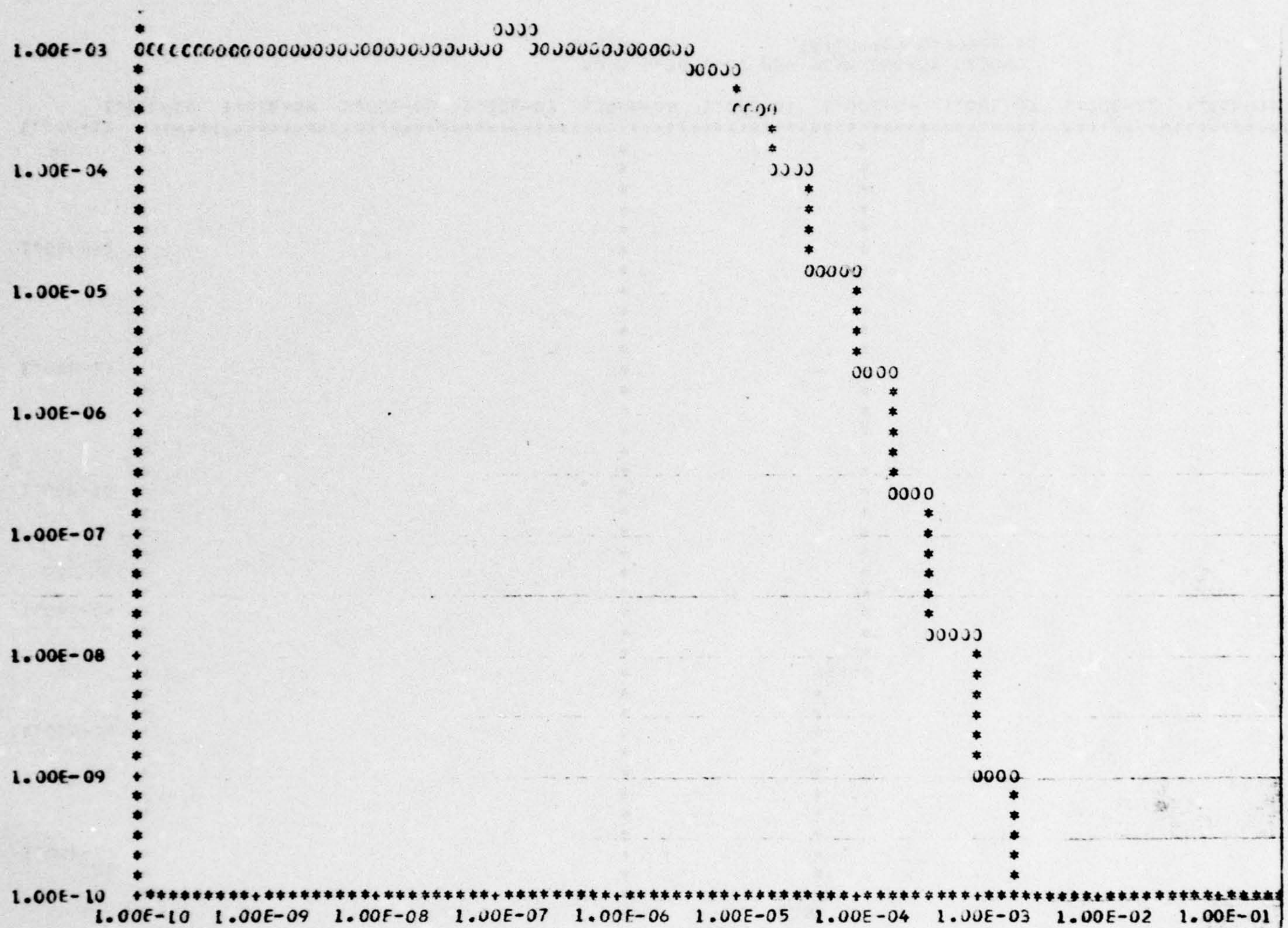

HDL3 50 M 1.11-0.55 MEV NEUTRONS

FIGURE 23 REGION 1 INTEGRAL= 0.1857E-07

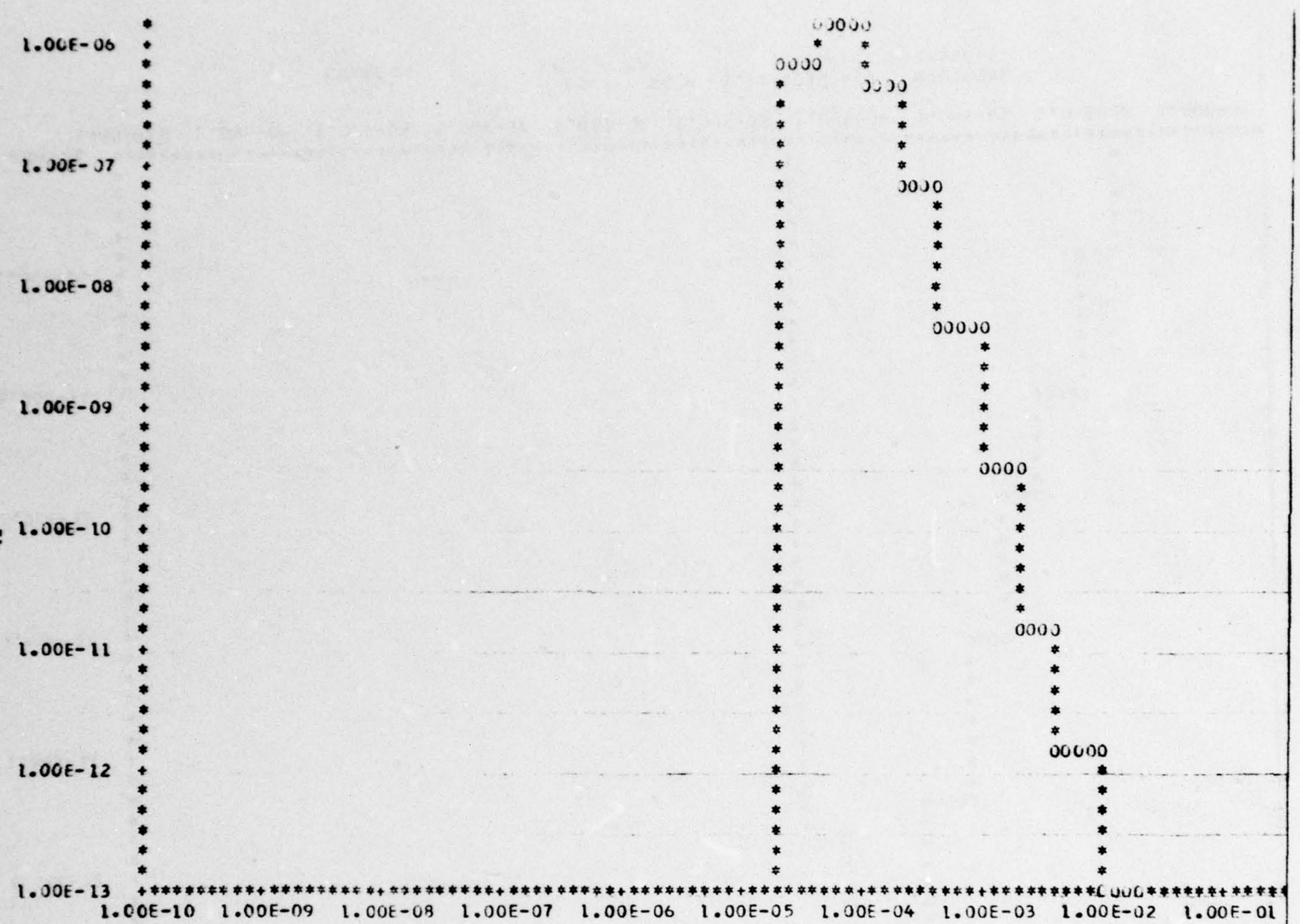

FIGURE 24 HDL3 50 M 1.11-0.55 MEV NEUTRONS
REGION 17 INTEGRAL= 0.1930E-09

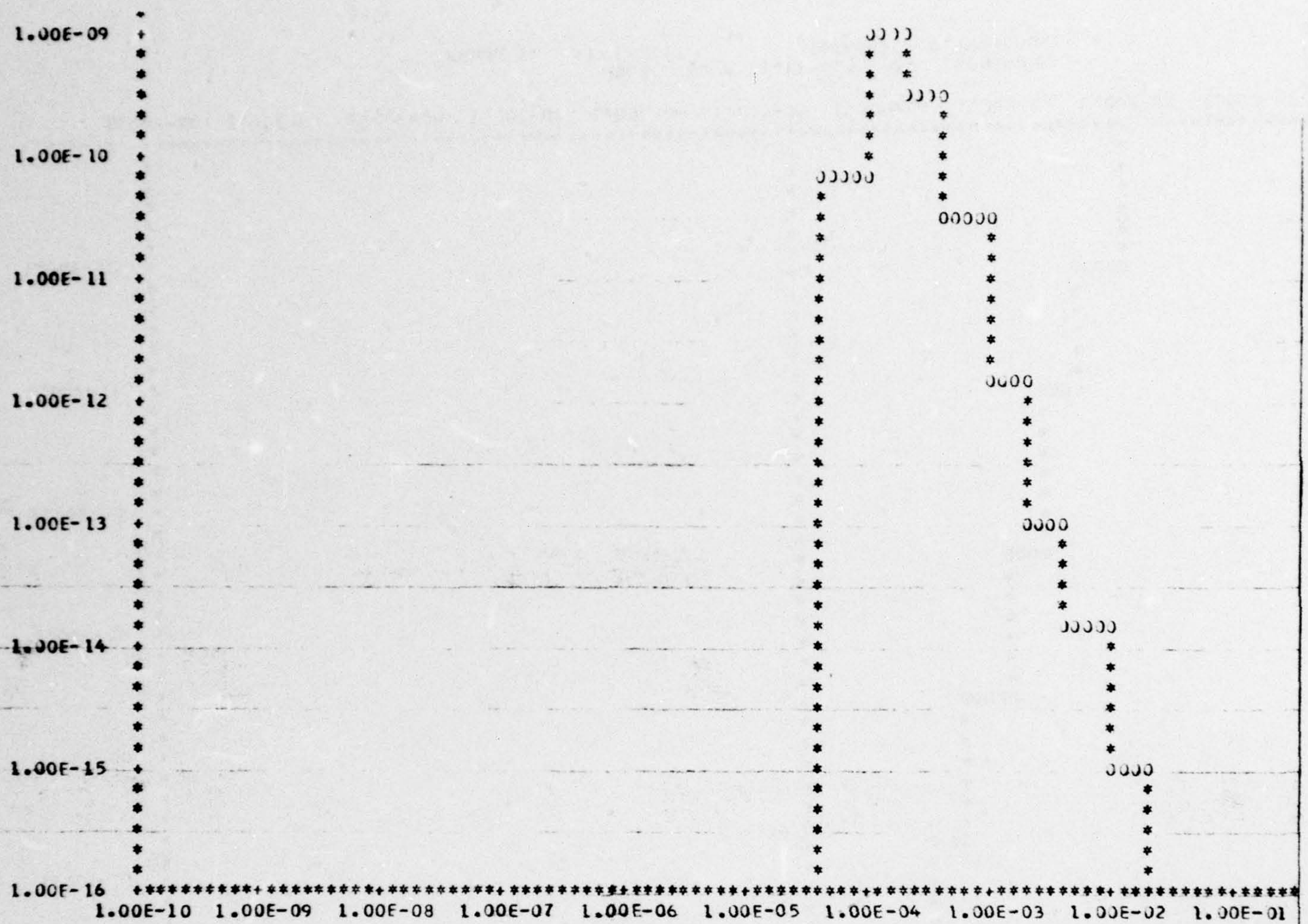

FIGURE 25 HDL3 50 M 1.11-0.55 MEV NEUTRONS
REGION 32 INTEGRAL= 0.2750E-12

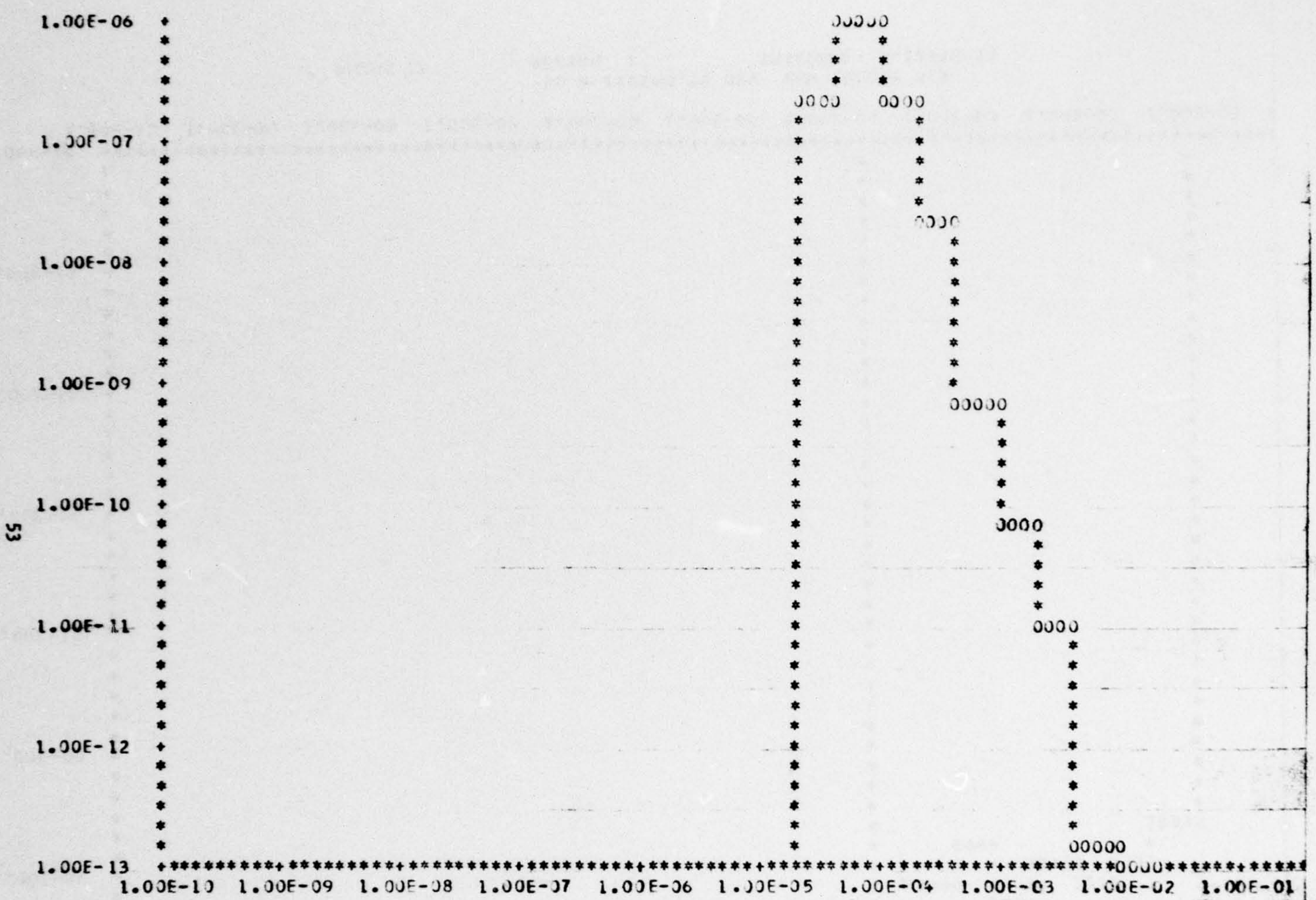

FIGURE 26

HDL3 50 M 1.11-0.55 MEV NEUTRONS
REGION 53 INTEGRAL= 0.9496E-10

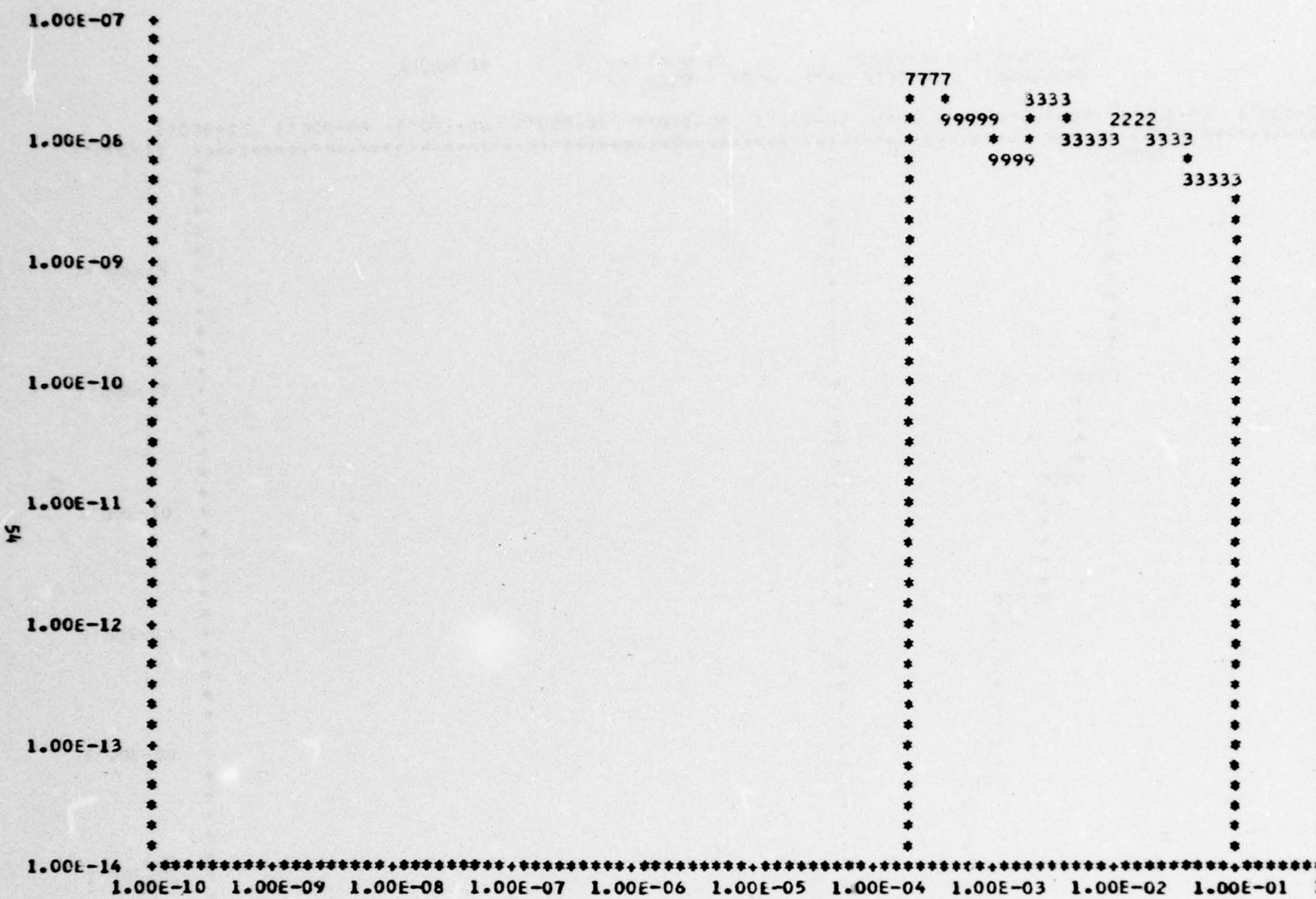

FIGURE 27

50 M 1.11-0.55 MEV LOW ENERGY AIR
REGION 1 INTEGRAL= 0.1034E-08

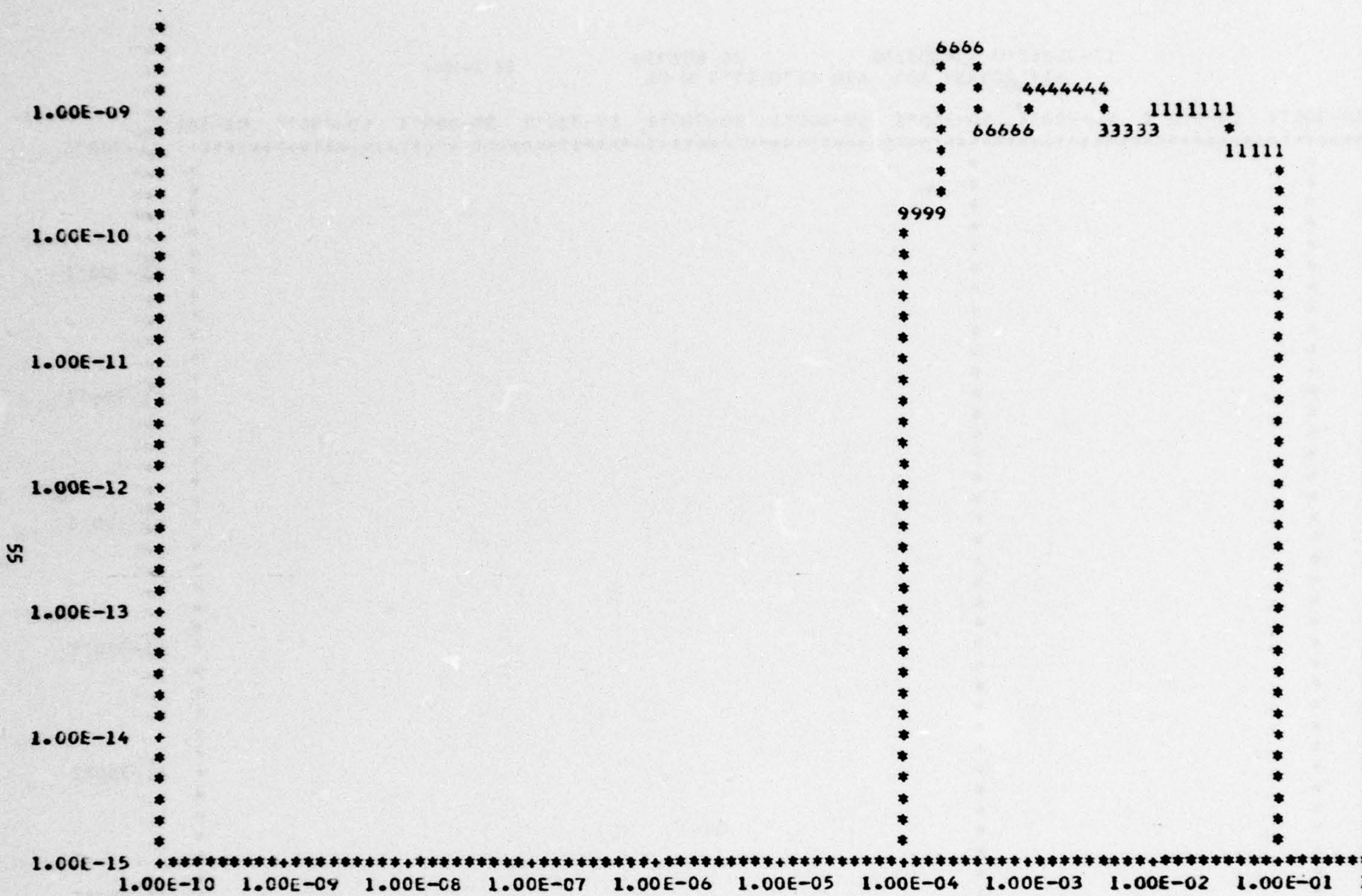

FIGURE 28

50 M 1.11-0.55 MEV LOW ENERGY AIR
REGION 17 INTEGRAL= 0.8943E-10

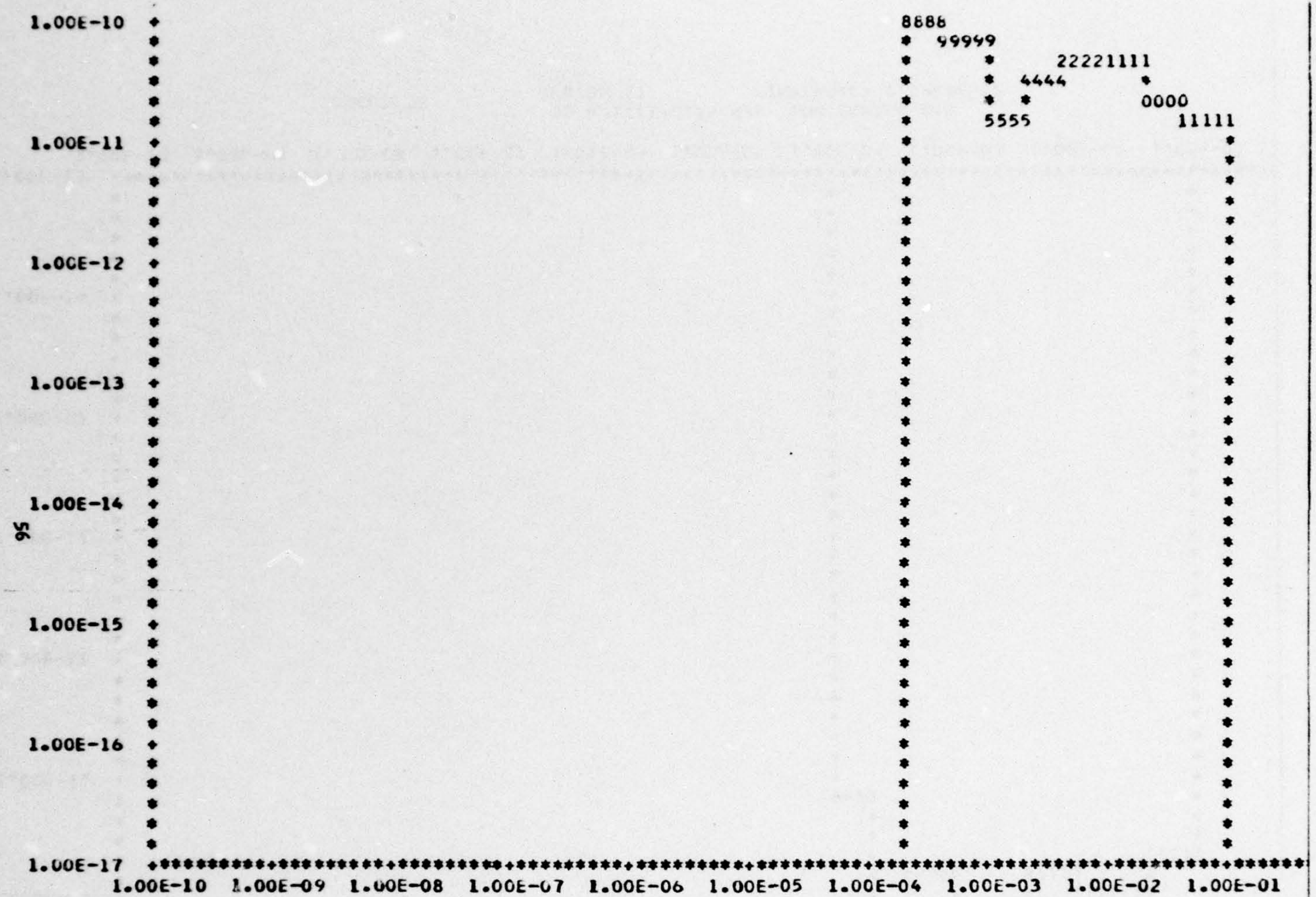

FIGURE 29

50 M 1.11-0.55 MEV LOW ENERGY AIR
REGION 32 INTEGRAL= 0.2925E-11

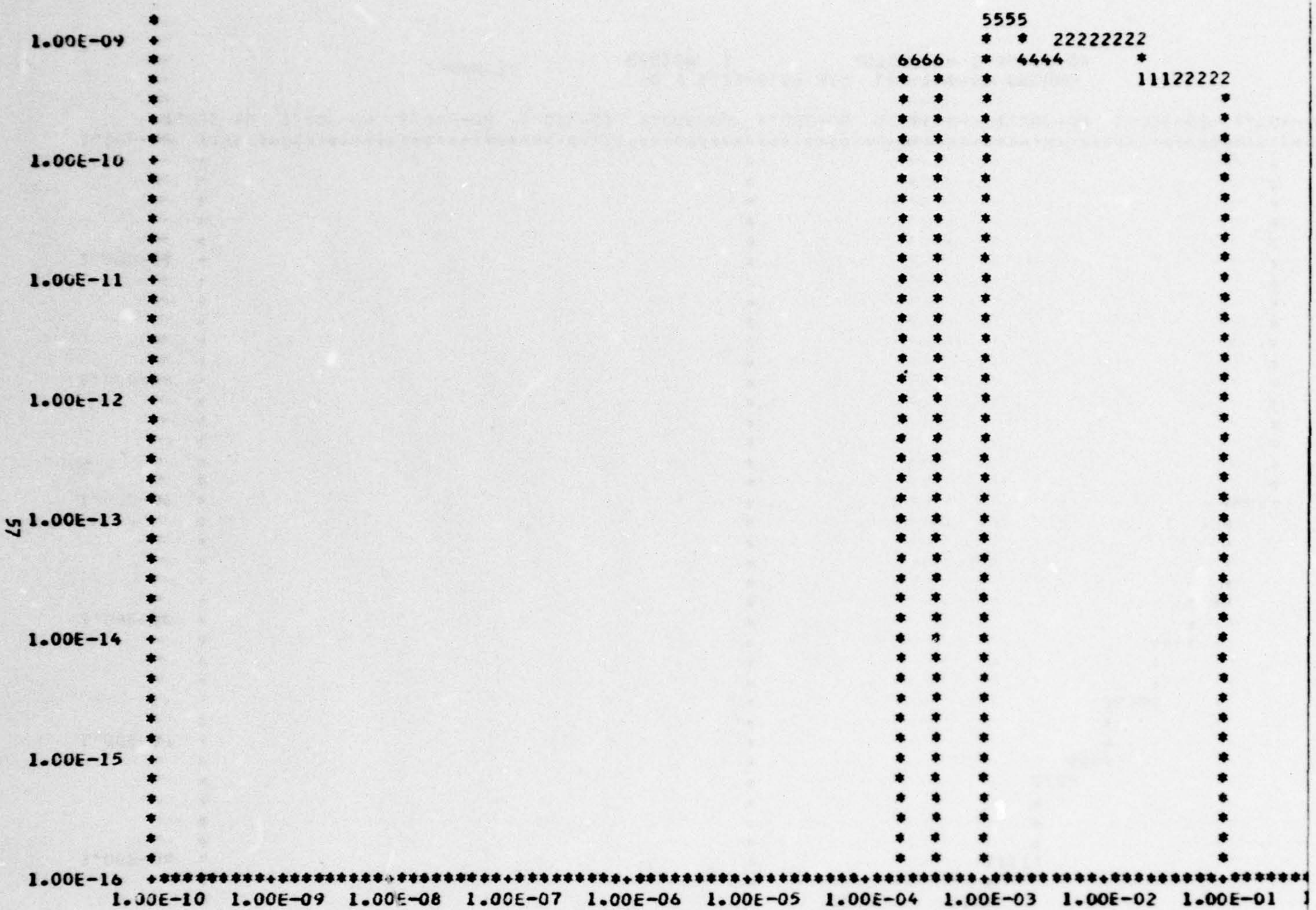

FIGURE 30 50 M 1.11-0.55 MEV LOW ENERGY AIR
REGION 53 INTEGRAL= 0.6469E-10

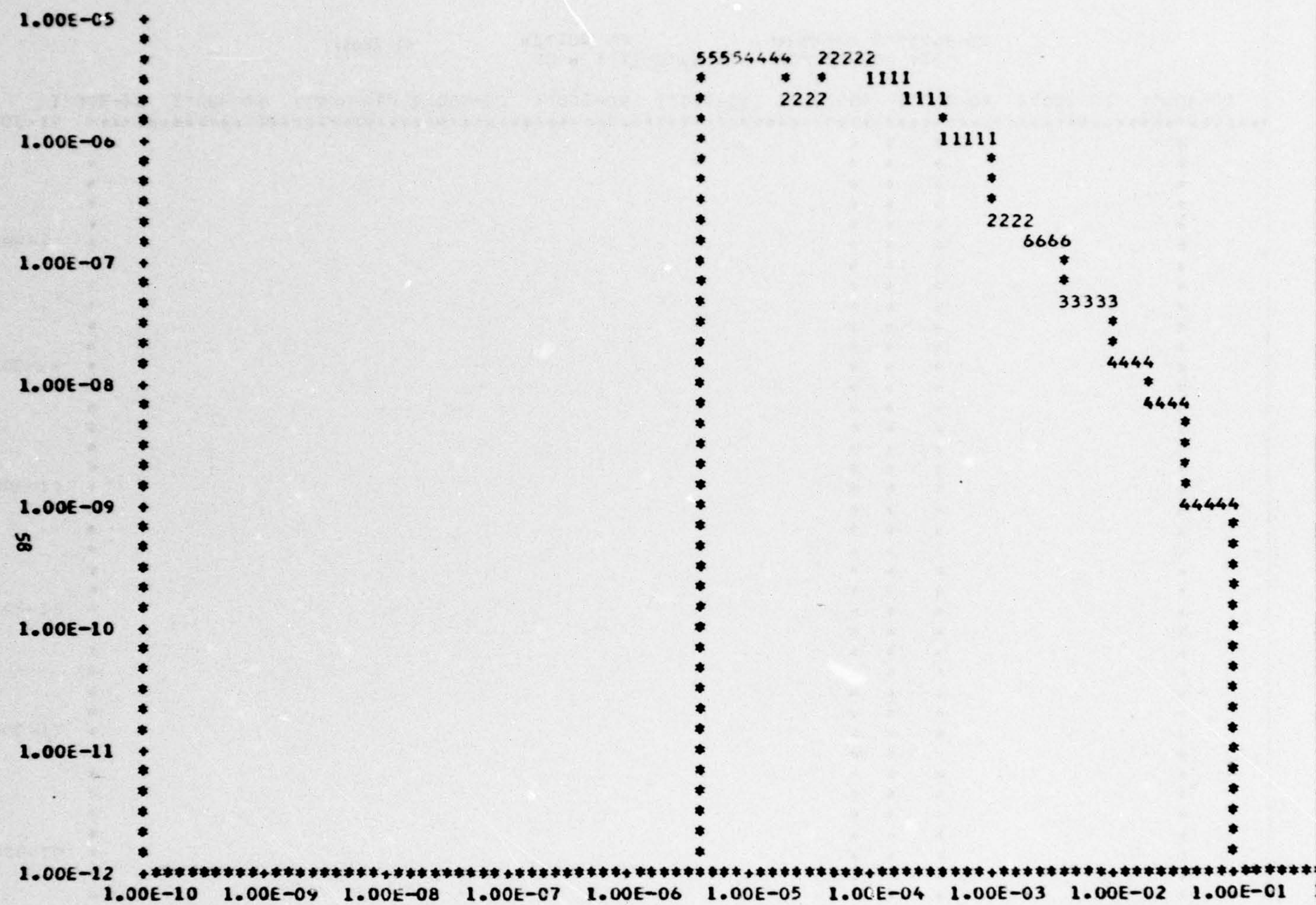

FIGURE 31

50 M 1.11-0.55 MEV LOW ENERGY GROUND
REGION 1 INTEGRAL= 0.3640E-08

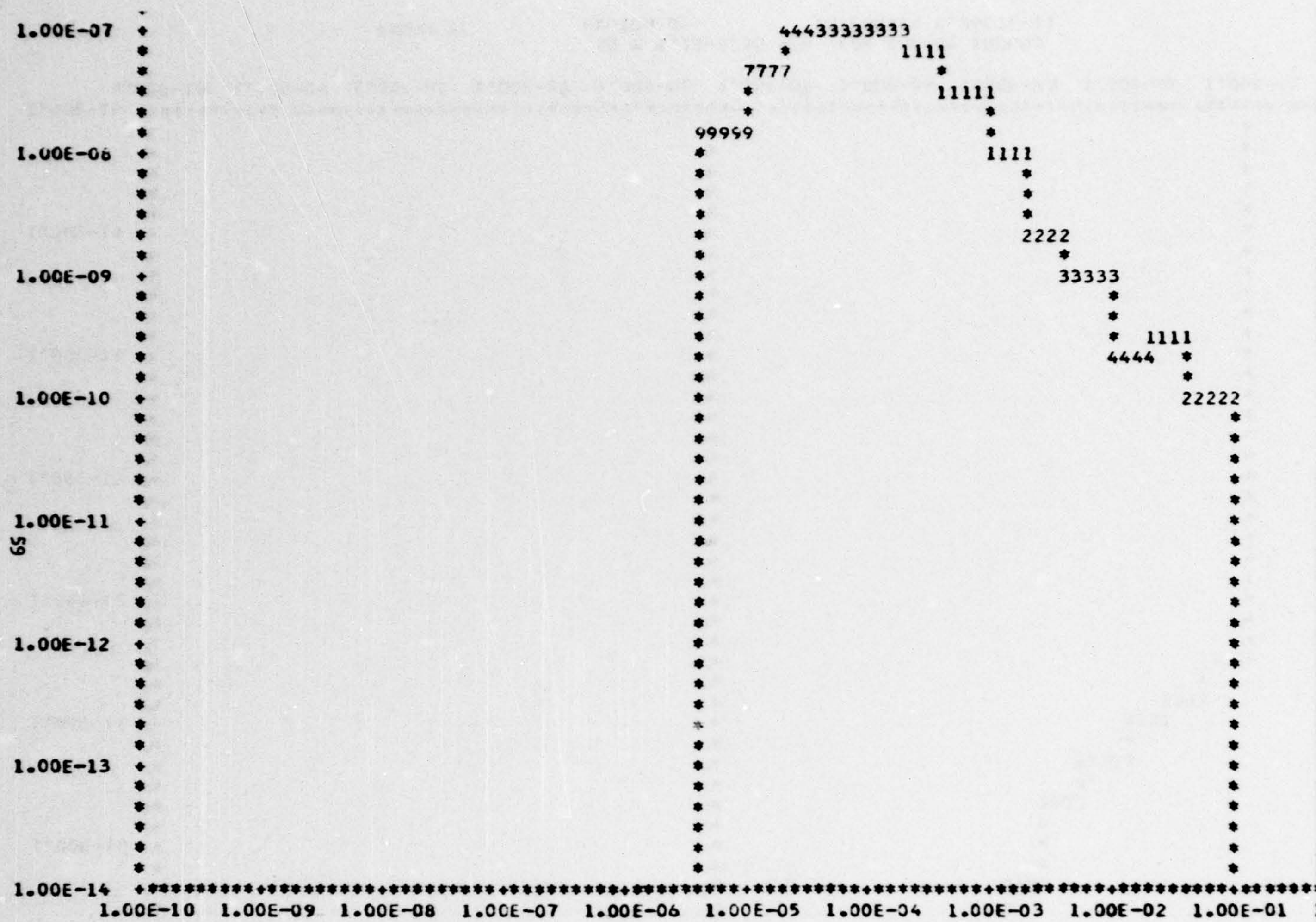

FIGURE 32

50 M 1.11-0.55 MEV LOW ENERGY GROUND
REGION 17 INTEGRAL= 0.1063E-09

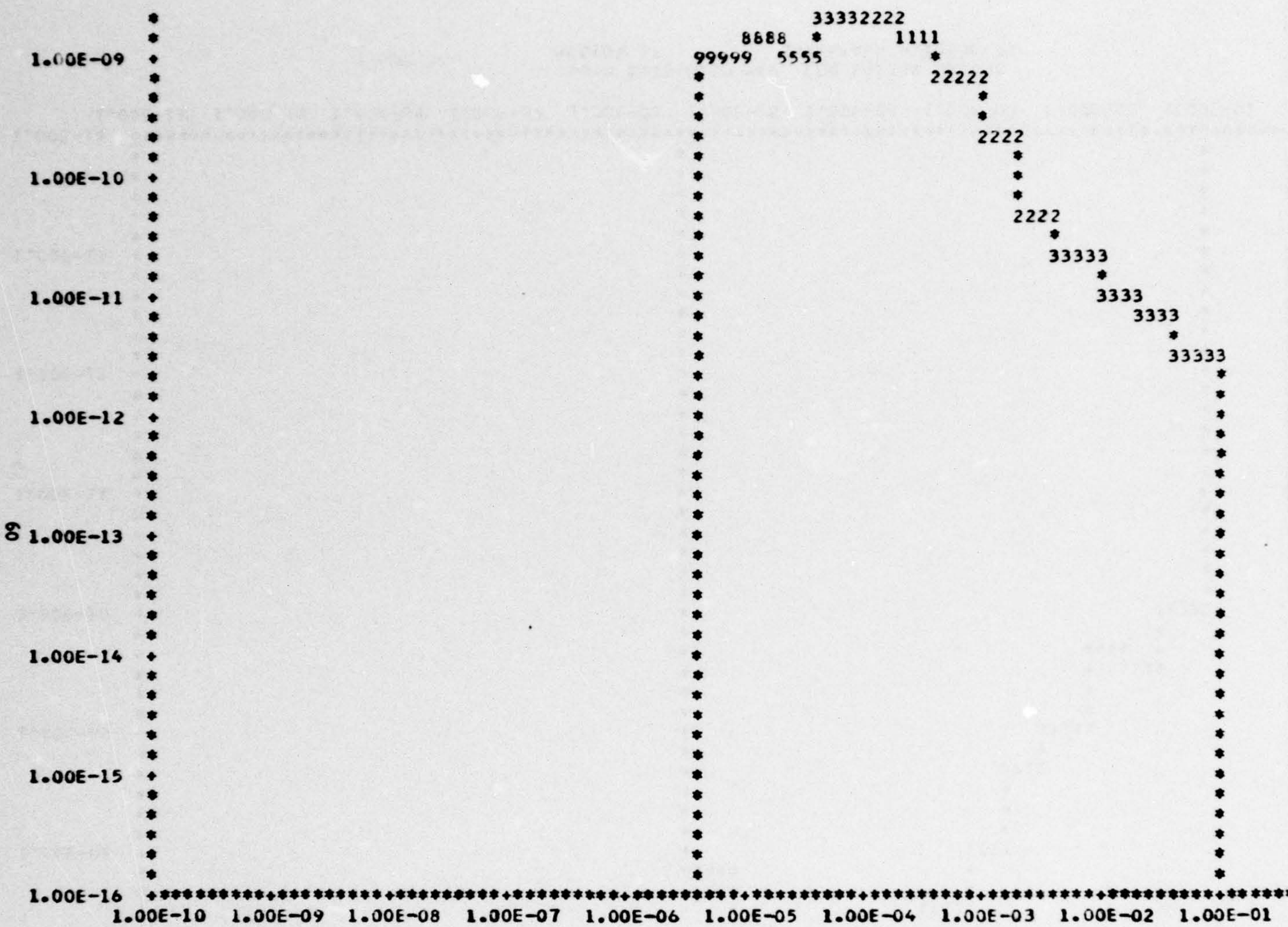

FIGURE 33 50 M 1.11-0.55 MEV LOW ENERGY GROUND
REGION 32 INTEGRAL= 0.2607E-11

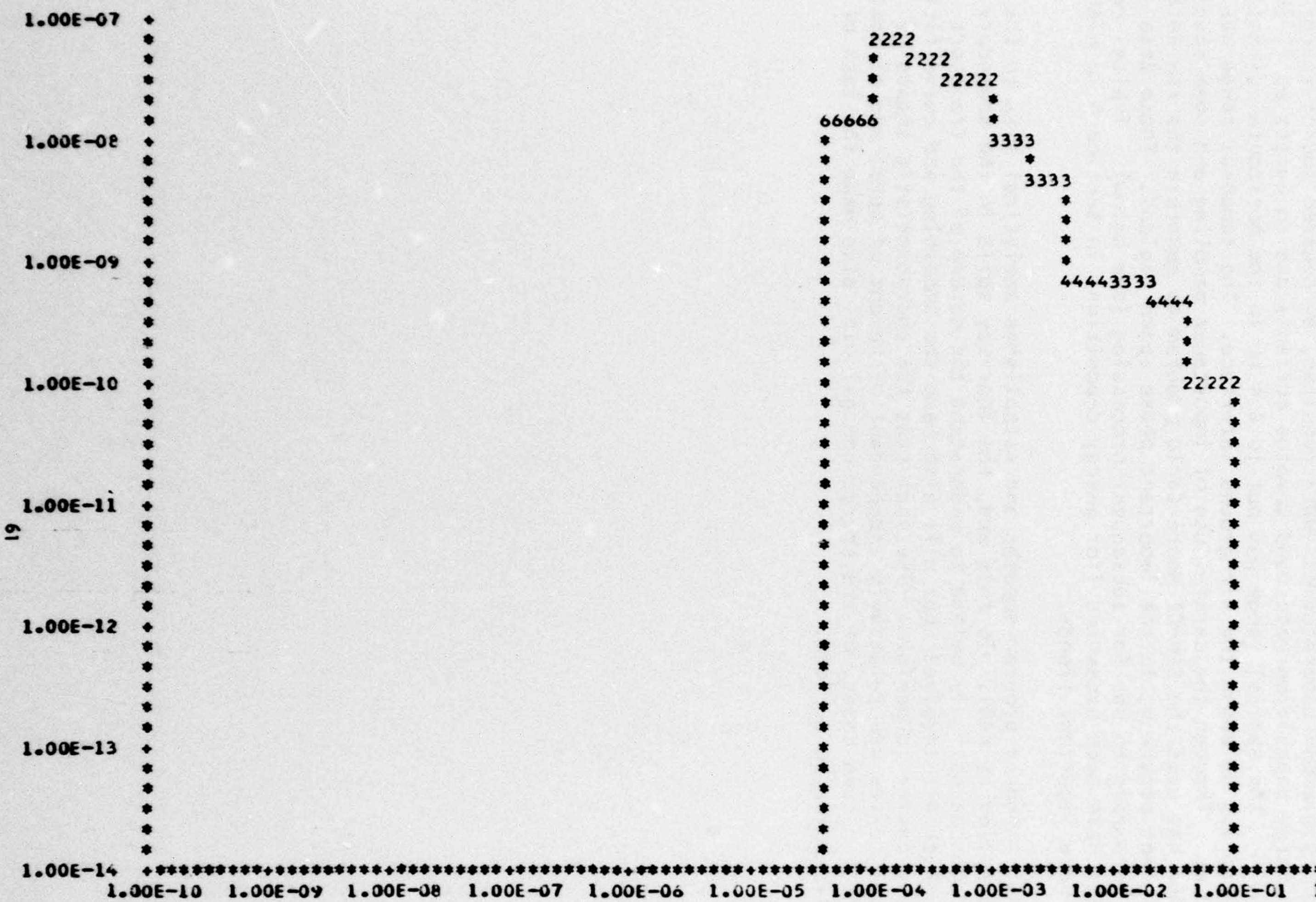

FIGURE 34

50 M 1.11-0.55 MEV LOW ENERGY GROUND
REGION 53 INTEGRAL= 0.1092E-09

5. CONCLUSIONS

The Harry Diamond Laboratories (HDL) required, by neutron source energy band, the energy deposition rates and Compton currents due to bursts at 1, 50, 100 and 200 m. The spatial range was out to 2.4 km in the horizontal direction and from 0 to 1.5 km above the air-ground interface. The temporal range was out to 100 ms. Through the careful use of importance sampling and some special coding, MAGI has used the SAM-CE Monte Carlo program to generate the raw data, with sufficient accuracy, in the important phase space regions. These data have been forwarded to HDL for subsequent processing (see below). Typical raw data results have been presented (for energy deposition) in Section 4 to highlight the more important trends.

The HDL in-house program smooths and establishes analytical fits to the raw data supplied by MAGI. To this end, the four-way split in the secondary gamma-ray sources not only helped to understand the nature of the transport processes which are involved, but will also make the smoothing and curve fitting considerably easier to perform. The fact that the characteristic shapes of the temporal curves are relatively independent of height of burst and of spatial region (and, in some cases, of the source energy) will also make the task of HDL notably easier to perform.

DISTRIBUTION LIST

	COPIES
Defense Documentation Center ATTN: DDC-TCA Cameron Station, Building 5 Alexandria, VA 22314	12
Director Defense Nuclear Agency Washington, D.C. 20305	
ATTN: STSI	1
ATTN: STRA	1
ATTN: STTL	1
ATTN: RAEV (CPT W. Wilson)	1
Commander Harry Diamond Laboratories 2800 Powder Mill Road Adelphi, MD 20783	
ATTN: DELHD-TI, Tech. Lib.	3
ATTN: DELHD-EMC, William T. Wyatt, Jr.	3
ATTN: DELHD-EMC, Daniel J. Spohn	1
ATTN: DELHD-NP, Francis N. Wimenitz	1
ATTN: DELHD-NP, Sy Moazed	1
ATTN: DELHD-TIC	1
ATTN: DELHD-ASA (Record Copy)	1
ATTN: DELHD-TI, Editorial Committee	1
Director US Army Ballistic Research Laboratories ATTN: DRXBR-AM, Dr. N. E. Banks Aberdeen Proving Ground, MD 21005	1
Commander Naval Surface Weapons Center White Oak Laboratory Silver Spring, MD 20910	
ATTN: Code WA-501, Navy Nuc. Prgms. Offc.	1
ATTN: Code WA-50, Dr. John H. Malloy	1
ATTN: Code WX-21, Tech. Lib.	1
Commander Air Force Weapons Laboratory, AFSC Kirtland Air Force Base, NM 87117	
ATTN: ELP, Dr. William Page	1
ATTN: EL, Dr. John Darrah	1
ATTN: ELP, Dr. Carl E. Baum	1
ATTN: EL, Library	1

	COPIES
University of California Lawrence Livermore Laboratory P.O. Box 808 Livermore, CA 94551 ATTN: Dr. Louis F. Wouters	1
Los Alamos Scientific Laboratory ATTN: Document Control for Dr. John S. Malik Los Alamos, NM 87544	1
Mission Research Corporation P.O. Drawer 719 Santa Barbara, CA 93102	
ATTN: William C. Hart	1
ATTN: Dr. H. J. Longley	1
ATTN: Dr. Conrad L. Longmire	1
ATTN: Technical Library	1
R&D Associates ATTN: R. R. Schaefer P.O. Box 3580 Santa Monica, CA 90403	1
General Electric Company TEMPO-Center for Advanced Studies ATTN: DASIAC 816 State St. Santa Barbara, CA 93102	1
JAYCOR, Inc. ATTN: William A. Radasky 1401 Camino Del Mar Del Mar, CA 92014	1
Mathematical Applications Group, Inc. 3 Westchester Plaza Elmsford, NY 10523	
ATTN: M. O. Cohen	1
	1
Dr. Paul N. Stevens Dept of Nuclear Engineering University of Tennessee Knoxville, TN 22193	1
Radiation Shielding Information Center Oak Ridge National Laboratory Post Office Box X Oak Ridge, TN 37830	2